Ore Geology Reviews xxx (2017) xxx–xxx

Contents lists available at ScienceDirect

Ore Geology Reviews

journal homepage: www.elsevier.com/locate/oregeo

Textural development in sulfide-matrix ore breccias in the Voisey's Bay Ni-Cu-Co deposit, Labrador, Canada

Stephen J. Barnes [a,*], Margaux Le Vaillant [a], Peter C. Lightfoot [b]

[a] CSIRO Mineral Resources, Perth, Australia
[b] Lightfoot Geoscience Inc, Sudbury, Canada

ARTICLE INFO

Article history:
Received 11 November 2016
Received in revised form 12 March 2017
Accepted 20 March 2017
Available online xxxx
For OGR special issue, 13th International Ni-Cu-PGE Symposium

Keywords:
Nickel
Magmatic sulfide
Intrusion
Emplacement
Infiltration
Percolation

ABSTRACT

Magmatic Ni-Cu sulfide ores at Voisey's Bay contain complex assemblages of extremely heterogeneous rocks. These range from polymict breccias, with rock fragments in sulfide-rich and/or sulfide-poor matrices, to heterogeneous "vari-textured" gabbros with rapid short range variations in grain size and content of hydrous phases. Rock fragment populations in the breccias include endogenous olivine gabbros (cumulate and non-cumulate) and cumulate peridotites along with extensively depleted plagioclase-hercynite gneisses interpreted as restites from extensive partial melting of country rock quartzo-feldspathic paragneisses. Using a combination of desk-top microbeam XRF mapping at cm scale and 3D X-ray tomography, we show that both sulfide-poor and sulfide-rich breccias comprise heterolithic assemblages of clasts within a matrix of olivine gabbro. This matrix is characterised by an interconnected 3D framework of plagioclase crystals, highly variable in grain size at mm to cm scale, with interstitial olivine and poikilitic clinopyroxene, and is texturally indistinguishable from clast-free olivine gabbro. Sulfide forms interconnected networks at cm to dm scale and possibly larger. Much of the plagioclase developed by outgrowth from the margins of paragneiss xenoliths when the porosity was occupied by silicate melt. The observed range of textures is explained by a model of percolation of molten sulfide through variably crystalline inter-clast matrix, displacing the silicate melt to leave the refractory plagioclase-olivine or in some cases plagioclase-only component, now entirely within a sulfide matrix. The process is analogous to that believed to have formed interspinifex ore in komatiite-hosted deposits. Biotite rims on plagioclase enclosed in sulfide are interpreted as the result of reaction between plagioclase, olivine and a hydrous component derived from the sulfide melt itself, with a possible component of migrating residual silicate melt wicking along sulfide-silicate contacts. This sulfide infiltration model offers an alternative to the current model for upward emplacement of a slurry of silicate melt, sulfide melt and breccia fragments as a late stage injection into the dyke-sill complex. The preserved range of textures is interpreted as being due to gravity-driven percolation of sulfide liquid through a pre-existing partially molten intrusion breccia. In this model, the breccia serves as a physical trap site, accumulating downward migrating sulfide liquid. However, the invariable close mutual association of sulfide and rock fragments at Voisey's Bay implies a common derivation.

1. Introduction

Magmatic Ni-Cu-PGE sulfide ores are marked by a wide diversity of textural types that provide important clues to their origin. Ores hosted in small mafic-ultramafic conduit-style intrusions commonly contain a high proportion of sulfide-matrix breccias, by which we mean assemblages of silicate rock fragments within a matrix of original magmatic sulfide liquid. Such ore types have been widely recognised and reported, but with a few exceptions (Ripley and Alawi, 1988; Arcuri et al., 1998; Li and Naldrett, 2000; Mariga et al., 2006b,a; Pina et al., 2006; Samalens et al., 2016) have received little in the way of detailed study. This contribution forms part of an ongoing investigation of magmatic sulfide textures (Barnes et al., 2016a, 2017; Staude et al., 2016, 2017) aiming to establish a coherent set of genetic models, based on a sound understanding of the physics as well as the chemistry, that account for the spectrum of observed ore types.

As a broad generalisation, sulfide matrix breccia ores are characteristic of deposits formed from mafic host magmas, but are less prevalent in komatiite hosted deposits. Variably textured mafic

* Corresponding author.
E-mail address: steve.barnes@csiro.au (S.J. Barnes).

http://dx.doi.org/10.1016/j.oregeorev.2017.03.019
0169-1368/© 2017 Elsevier B.V. All rights reserved.

rocks with large irregular short range variation in grain size, referred to in different places as "vari-textured" (Voisey's Bay) or "taxitic" (Siberia), and commonly containing partially digested xenoliths, are likewise a widespread feature of mafic-hosted systems. They are commonly associated with sulfide-matrix breccia ores, in some cases being completely mutually gradational.

Detailed investigations of ore textures from a large number of deposits is however revealing more commonality between ultramafic and mafic hosted systems. Country-rock inclusions are locally abundant in some komatiite-hosted deposits, e.g. Digger Rocks and Silver Swan in Western Australia and Hunter Road in Zimbabwe (Perring et al., 1995; Prendergast, 2001; Dowling et al., 2004), as well as in mafic systems, and (as we show here) net-textured ores can be found in mafic systems, albeit with somewhat different silicate mineralogy, as well as in komatiites. At Sudbury, both exotic inclusions, and inclusions derived from adjacent country rocks are common, and they are dominantly of mafic-ultramafic composition, with very rare examples of metasedimentary rock or granite-gneiss despite the volumetric importance of this type of country rock (Lightfoot, 2016).

A particularly distinctive suite of sulfide matrix breccias is present in the Voisey's Bay deposits in Labrador, Canada (Evans-Lamswood et al., 2000; Li and Naldrett, 2000). The Voisey's Bay ore system comprises a series of massive, disseminated and breccia-textured ores hosted within various components of a structurally-controlled sill-dyke complex (Naldrett et al., 2000; Ripley and Li, 2011; Lightfoot et al., 2012; Saumur et al., 2013, 2015; Lightfoot and Evans-Lamswood, 2015; Saumur and Cruden, 2015). Massive ores are characteristically fringed by breccia textured ores and sulfidic taxites (referred to as "vari-textured troctolites" at Voisey's Bay), and there is a very close association between sulfide concentrations and presence of breccias. Unlike some localities, where the magmatic as opposed to tectonic origin of sulfide-matrix ore breccias is ambiguous, much of the Voisey's Bay breccia-textured ore assemblage, including all of the samples investigated in this study, preserve extremely delicate igneous textures and are undeniably magmatic, making it an ideal case study.

Here we make extensive use of the technique of desk-top microbeam XRF mapping (Barnes et al., 2016c), combined with 3D X-ray tomography using a standard medical CT scanner (Godel et al., 2006), to reveal petrographic features, textures and chemical zoning patterns in Voisey's Bay ores at a scale of centimeters to decimetres. This scale is intermediate between the microscopic thin-section scale and the drill core/outcrop to mine scale at which geological relationships are most commonly viewed, and provides a method of visualizing the distribution of clasts types, sulfides and accessory minerals in a very informative way.

2. Geological setting

The 1.34 Ga Voisey's Bay Intrusion is located within the central part of the Nain Plutonic Suite in Labrador, north-eastern Canada, astride the boundary between Paleoproterozoic-aged Churchill paragneiss and enderbitic orthogneiss to the west and Archean orthogneiss of the Nain Craton to the east (Ryan, 2000). The intrusion is localized within a major east-west structural corridor where early dextral displacement coupled with extension created space into which the mafic magmas and ore deposits were emplaced. The same structures underwent sinistral deformation after the emplacement of younger mafic intrusions of the Nain Plutonic Suite such as the Mushuau Intrusion (Lightfoot et al., 2012; Saumur et al., 2015; Lightfoot and Evans-Lamswood, 2015). The corridors created by deformation at the time of Nain Plutonic Suite magmatism played an important part in controlling the intrusions and ore deposits.

The Voisey's Bay Intrusion consists of two tabular chambers comprising weakly differentiated units of troctolite, augite troctolite, olivine gabbro, and gabbro that contain many hanging pendants of country rock gneisses within the stratigraphy. The easternmost intrusion is extensively explored; the Eastern Deeps magmatic Ni-Cu-Co sulfide ore deposit is localized at the base of the Eastern Deeps chamber proximal to the entry point of a gently dipping dyke into the northern base of the intrusion (Fig. 1; Naldrett et al., 1996; Lightfoot et al., 2012). The Eastern Deeps ore deposit consists of a series of thick lenses of massive sulfide with up to 10% magnetite that reside within a sequence of inclusion-rich variable textured troctolites and olivine gabbros with up to 50% sulfide, termed the basal breccia sequence (Naldrett et al., 1996). The breccia sequence rocks and massive sulfides are overlain by a mound-shaped body of vari-textured troctolite hosting massive, semi-massive and disseminated sulfide that contains <5% inclusions and 0–25% sulfide in rocks ranging from fine-grained through to pegmatoidal textures (Fig. 2). This body of vari-textured troctolite abuts the northern margin of the Eastern deeps chamber and thins towards the south where the massive sulfide and breccia sequence of the Eastern Deeps deposit pinches out (Fig. 2). The dyke to the north of the Eastern Deeps consists of ferrodiorite, ferrogabbro, and olivine gabbro at the margin and a core of variable troctolite with discontinuous domains of sub-economic magmatic sulfide mineralization (Lightfoot and Evans-Lamswood, 2015). The mineralization contained in the dyke becomes thicker as the dyke connects into the Eastern Deeps chamber, and the mineral zone is contiguous with the Eastern Deeps Deposit.

The base of the Eastern Deeps intrusion dips at 20 degrees towards the east and sub-crops in a zone of disseminated sulfide mineralization termed the Southeastern Extension. Further to the west the dyke that links into the chamber disappears and a second sub-parallel dyke joins with a bowl-shaped body of massive sulfide and breccia sequence rocks that is termed the Ovoid. The Ovoid deposit is marked by the development of massive pyrrhotite, chalcopyrite, and pentlandite with up to 25% magnetite (Huminicki et al., 2012). The massive sulfides exhibit a sharp contact with the breccia sequence and more weakly mineralized variable-textured troctolite. The edges of the Ovoid comprise ferrodiorite, ferrogabbro, and olivine gabbro (Lightfoot et al., 2012). The dyke which connects to the base of the Ovoid has a core of mineralized vari-textured troctolite which extends for several hundred metres beneath the Ovoid as a discontinuous sub-economic mineralized zone.

To the west of the Ovoid, a second mineralized zone is developed as the bowl-shaped geometry of the Ovoid narrows into a dyke-like form (Fig. 1a). This deposit is termed the Mini-Ovoid, and it is contiguous with the Ovoid, but has a slightly different sulfide geochemistry when compared to the Ovoid (Lightfoot et al., 2012). The root of the Mini-Ovoid comprises rock types and mineralization similar to that developed in the Ovoid dyke. Further to the west, the intrusion narrows into a dyke geometry. The Discovery Hill mineralized zone is contained within this dyke, and principally consists of inclusion-rich variable-textured troctolite and olivine gabbro with up to 50% sulfide. This mineral zone plunges down the dyke towards the east at an angle of 45 degrees, and is open at depth (Fig. 1).

Further to the east, two other domains of mineralization are associated with the Reid Brook extension of the dyke. These zones comprise dyke-hosted massive sulfide veins, breccia sequence sulfides, and disseminated sulfides in rock types similar to those found in the Ovoid dyke. The dyke geometry is discontinuous with gently plunging structures localizing the development of massive sulfide veins in the adjacent country rock paragneiss. These two sulfide types have similar geochemistry despite the very different host rocks.

Please cite this article in press as: Barnes, S.J., et al. Textural development in sulfide-matrix ore breccias in the Voisey's Bay Ni-Cu-Co deposit, Labrador, Canada. Ore Geology Reviews (2017), http://dx.doi.org/10.1016/j.oregeorev.2017.03.019

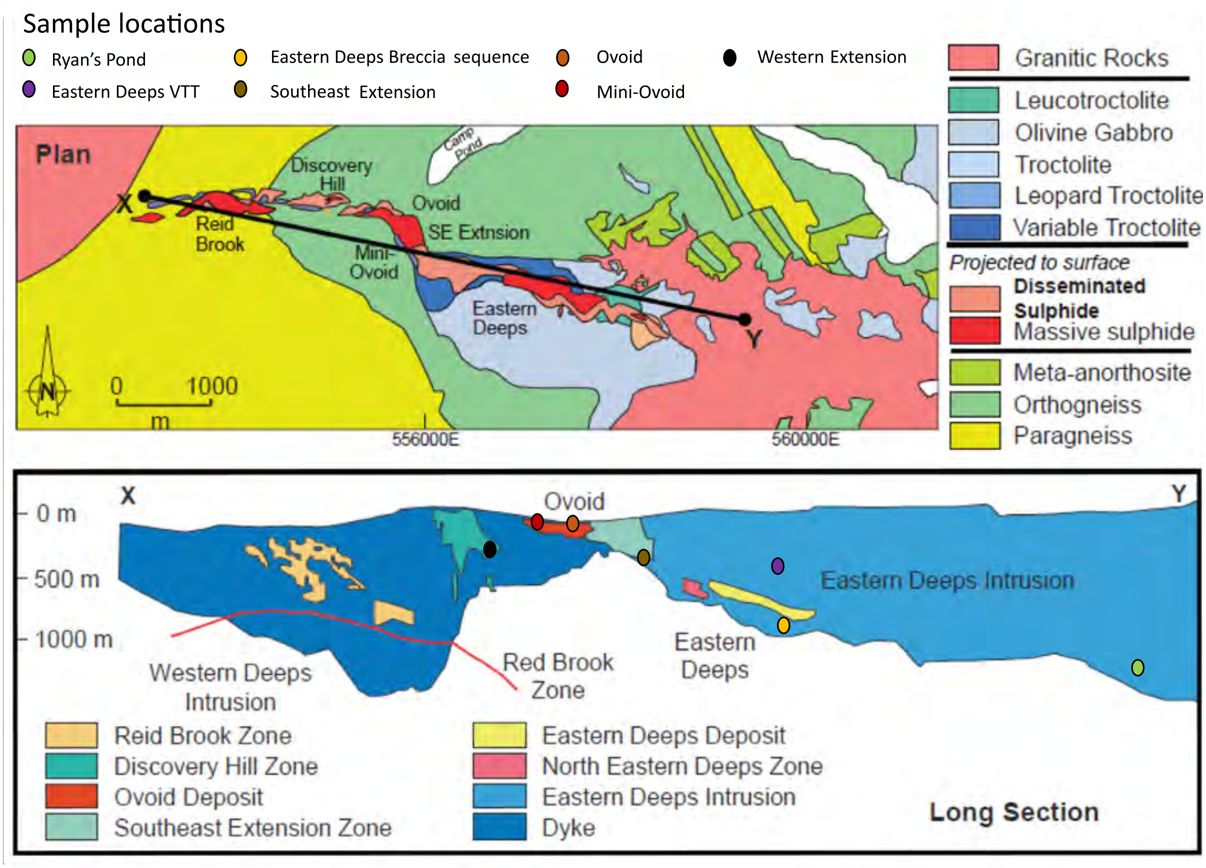

Fig. 1. A. Geological map of the Voisey's Bay Intrusion (a) showing the location of a WNW-ESE long section (b). Long section (b) shows the projected geometry of the Eastern deeps, Western Sub-chamber, and Reid Brook Dyke; superimposed are the locations of the clusters of samples collected from west to east across the deposit. The three principal zones of mineralization rake down the dyke with a plunge of about 45°. The mineral zones are shown as grade shells generated by implicit modelling.

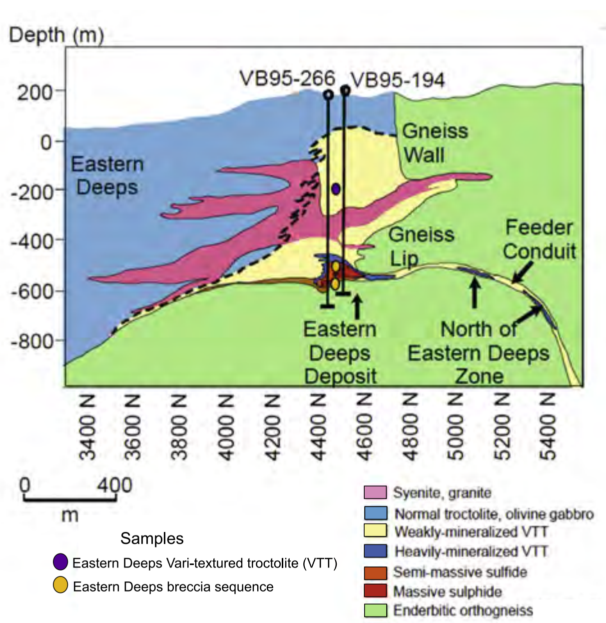

Fig. 2. Projected N-S geological section through the Eastern deeps Deposit, showing the location of samples taken above and below the massive sulfide ore body. Based on Lightfoot et al. (2012). Dashed line shows the mineralization envelope.

Throughout the deposit, the economically important styles of mineralization group as: 1, massive sulfide with very rare inclusions or silicate segregations, and up to 25% magnetite; and 2, sulfide matrix breccias (locally referred to as breccia sequence sulfides) that comprise fragments of paragneiss and endogenously-derived olivine gabbros and peridotites within a matrix of olivine gabbro and troctolite. Disseminated types of sulfide mineralization are hosted in variable-textured troctolite and olivine gabbro that forms a broad halo over the economically important sulfides of the Eastern Deeps. These rocks locally have a different sulfide metal tenor when compared to the massive and breccia sequence sulfides (Lightfoot et al., 2012).

2.1. Silicate inclusions in Voisey's Bay ore breccias

The petrology of gneissic inclusions in the Voisey's Bay breccias has been described in detail by Li and Naldrett (2000) and Mariga et al. (2006a,b). These authors identify three major lithological types, all occurring within a matrix of variably sulfide-rich troctolite and gabbro: paragneisses, consisting of assemblages of anorthitic plagioclase, corundum, hercynite, garnet (replaced by hercynite) and magnetite; olivine-bearing ultramafic rocks, usually feldspathic olivine-rich cumulates; and less abundant troctolite and gabbro. The paragneiss xenoliths, typically of the order of a few cm in size, show various forms of concentric zoning defined primarily by varying proportions of hercynite, corundum and milky plagioclase. The paragneiss inclusions according to Li and Naldrett (2000) represent widely varying degrees of reaction with the enclosing magma, the extremely aluminous hercynite and corundum rich varieties being the most extensively reacted. Hercynite-bearing clasts are typically rimmed by 1–3 mm intergrowths of biotite-phlogopite (referred to as biotite hereafter for simplicity) and highly calcic plagioclase that decreases in An content from centre to rim of the inclusions, with typical ranges from around An 60–70 in the cores to around An 50 in the rims. Many of the hercynite-plagioclase clasts are strongly banded and have platy geometries with high aspect ratios. Mariga et al. (2006a,b) conclude that the Reid Brook zone xenoliths are derived from immediate country rocks, pelitic Tasiuyak Gneiss, whereas xenoliths in the Eastern Deeps may be derived from the Tasiuyak Gneiss, various quartzo-feldspathic gneisses, or possibly enderbitic gneiss.

Mariga et al. (2006a,b) interpreted the hercynite-bearing paragneiss xenoliths as being the refractory remnants of extensive partial melt extraction into the transporting silicate melt, with diverse original lithologies evolving towards and converging on highly refractory residues with increasing melt extraction. This results in the formation of strongly peraluminous restites, predominantly anorthositic in composition, with development of hypersthene and corundum, and subsequent pseudomorphic replacement of corundum by hercynite, retaining original acicular and strongly prismatic crystal morphologies in the spinel aggregates. These features are clearly evident in the sample suite studied here. Lightfoot and Naldrett (1999) and Li et al. (2000) show that the Tasuiyak Gneiss falls at the end of a linear array of compositions of inclusion-bearing Voisey's Bay troctolites, while the local Nain gneisses and the country rock enderbites lie well off this trend. This strongly implies that the Tasuiyak gneiss is the main source of the paragneiss xenoliths, and further implies that these xenoliths were transported upwards, although a downward derivation from a now-eroded structurally overlying Tasuiyak gneiss source cannot be ruled out.

The paragneiss inclusions have aspect ratios of ~2:1 when incorporated in vari-textured troctolite. The ratio increases to ~5:1 to ~10:1 in the breccia sequence, and reaches ~100:1 in the "condensed breccia sequence" (Evans-Lamswood et al., 2000) in which the rocks exhibit some degree of shearing. These variants in morphology and the three different inclusion types are developed throughout the Voisey's Bay Deposit. The samples investigated here lack penetrative foliations or lineations or other evidence of post-emplacement tectonism.

In this contribution, relative to previous studies, we focus less on the xenoliths themselves and more on their relationship to the silicate and sulfide matrix that encloses them.

3. Methods and materials

A variety of imaging techniques has been used to illustrate sulfide-silicate textures. The main 2D imaging technique used in this study is that of X-ray fluorescence element mapping. Most of the maps (referred to hereafter as XRF maps) were generated by desktop microbeam XRF on the Bruker Tornado instrument at the CSIRO ARRC facility, Perth, at pixel sizes of 40 μm (Barnes et al., 2016a, 2016c). The unit is equipped with a rhodium target X-ray tube operating at 50 kV and 500 nA without filters and an XFlash VR silicon drift X-ray detector. Maps were created using a nominally 25 μm spot size on a 25–40 μm raster with dwell times of 10–20 ms per pixel. In addition a few 2–4 μm resolution images were collected using the Maia multi-detector array on the X-ray Fluorescence Microscopy (XFM) beamline of the Australian Synchrotron (Ryan et al., 2010, 2014; Paterson et al., 2011; Fisher et al., 2015). These are referred to below as XFM maps. The extent and morphology of sulfide aggregates is imaged by 3D X-ray computed tomography (XCT). Data are represented from low resolution (~mm scale) imaging using medical XCT scanning technology, on decimetre scale samples with coarse sulfide aggregates (Godel et al., 2006; Robertson et al., 2016). The Medical X-ray Computed Tomography system used for this study is a SOMATON Definition AS Medical CT Scanner housed at the CSIRO laboratories in Perth. This instrument is composed of a rotating X-ray source producing a fan-shaped X-ray beam, along with a rotating set of X-ray detectors (Multislice UFC™ detectors), and a 100 kW generator. The X-ray source is fitted with an STRATON MX P High Performance CT-X-ray tube, with intensity and voltage ranging from 20 to 800 mA and from 70 to 140 kV respectively, allowing the X-ray to be transmitted through dense and complex material such as disseminated to blebby magmatic Fe-Ni-Cu sulfides. Reconstruction to produce the tomographic dataset was done on the Syngo® Acquisition Workspace, and involves correction for anisotropic (non-cubic) voxel sizes. Further image processing was carried out using Azizo Fire™ software.

3.1. Visualisation of microbeam XRF element maps

As the technique of microbeam XRF mapping is still relatively new in the geoscientific literature, it is necessary to explain the protocols from deriving the false-colour three-element maps and derived phase distribution maps used in this paper. The three-element false colour maps are derived by scaling the X-ray count rates for each pixel to a user-defined minimum and maximum value for each selected element over the entire image, and assigning each of three selected elements to the red, green or blue channels of a 24-bit (8 bits, or 256 shades, per channel) RGB colour bitmap. This gives rise to distinctive colours for particular phases; for example, a map where S is assigned to red, Fe to green and Ca to blue would show pyrrhotite in yellow (combined red and green), olivine in pure green (Fe only, no S or Ca) and clinopyroxene in turquoise-blue (Ca > Fe, green + blue). In some cases, these maps can be used effectively to show distribution of phases, but in most cases it is necessary to use a larger number of elements to identify all the important phases in a sample. In these cases, phase maps were obtained in most cases by generating a number of different three-element maps, then using the colour selection wand tool in Adobe Photoshop™ image processing software to select and create colour masks attributable to particular phases. For most of the maps shown, we used combinations of S, Fe and Ca to define olivine, clinopyroxene and plagioclase; Ni, Cu and Fe to define pentlandite, pyrrhotite and chalcopyrite; and Ti, K and P to define ilmenite, biotite-phlogopite, and apatite. Separate legends are used on the various phase maps.

3.2. Samples

A total of 22 samples from drill core and from the Ovoid open pit, provided by Vale, were investigated in detail using desktop microbeam XRF mapping techniques, and 11 of these were also imaged in 3D. The samples were selected from the Western Extension, Mini-Ovoid, Ovoid, Southeastern Extension, and Eastern Deeps deposits as shown in Fig. 1B, to provide information about the textural relationships between silicate matrix, sulfide matrix, and inclusions (Fig. 1B). A full list of location data for all the samples imaged, grouped according to their principal location and geological environment, is given in the electronic supplement, and details of the samples illustrated in this paper are given in Table 1.

The samples record a range in inclusion content from inclusion-poor variable-textured troctolite which forms a halo around the Eastern Deeps deposit, through inclusion-rich vari-textured troctolite developed proximal to the deposit, and breccia sequence rocks that have both sulfide and silicate matrix, and occur directly adjacent to the massive sulfide mineralization. The samples also exhibit a range of sulfide contents from weakly disseminated sulfides

Table 1
Description of samples.

Sample name	Original Sample ID	Location	Stratigraphic group	Drill core	Depth (m)	Description	In paper
ED02	EDeeps-19	Eastern Deeps	Breccia sequence	VB95-194	720	Sulfide matrix breccia with herc-pg clasts(see paper)	Fig 10
ED03	ED-PL-BX1	Eastern Deeps	Vari-textured troctolite	VB95-194	724.5	Sulfide poor breccia - hghly "sloppy" Herc-Paragneiss xenos with very variable proportions of herc-bearing cores, distinct very clean sulfide patches with only minor plag laths at margins, small proportion of ol-gabbro matrix, irregular patches of v fine grained biotite-rich ?gabbro which may be highly contaminated ol-gabbro liquid?	Fig 13
ED04	FOG-VB95-205		Feeder dyke	VB95-205	213–237	Uniform-textured sulfide-poor olvine gabbro with cpx oikocrysts	Fig 3
ED10	VB-PL-EOL	Eastern Deeps	Breccia sequence	Grab sample		Coarse open-textured (but still clast supported) polymict sulfide-matrix breccia with large domains of poik olivine gabbro.	Fig 11
Ov01	VB-SB1-leopard	Mini-Ovoid	Vari-textured troctolite	Grab sample		Coarse to fine vari-textured troctolite with net-textured sulfide	Fig 5
Ov02	VB-ABSB1	Ovoid	Breccia sequence	Grab sample		Clast supported sulf-matrix breccia with mix of Hpg and ultramafic (olivine orthocumulate textured plag peridotite) clasts	Figs. 4 and 8
Ov03	ABSB1-bx-	Ovoid	Breccia sequence	Grab sample		Plag-rich "Leopard Ore" with large plag laths and relatively moinor olivine, no px, in sulfide matrix.	Fig 15
Ov05	VB-PL-OVOID-Bx2	Ovoid	Breccia sequence	Grab sample		Clast supported sulfide matrix breccia (Fig. BX2) showing four types of clasts: 1) ultramafic, consisting of olivine orthocumulate with interstitial plagioclase and clinopyroxene; 2) fine-grained troctolite; 3) strongly banded hercynite-anorthite paragneiss and 4) strongly zoned paragneiss clasts with aluminosilicate-rich, Ca poor cores and outer zones of hercynite-anorthite paragneiss.	Fig 6
Ov06	VB-PL-OVOID-Bx1	Ovoid	Breccia sequence	Grab sample		Xenolith-rich, biotite rich sulfide-poor, clast-supported intrusion breccia with extensively reacted clasts of nearly pure anorthosite, a few with hercynite-rich cores, in a continuous network matrix of poikilitic olivine gabbro and a population of Fe-rich clasts with extensive rimming by biotite.	Fig 13

from the halo above the Eastern Deeps through to semi-massive sulfides from the Ovoid. Samples of both fine-grained and coarse-grained troctolites were selected for this study.

4. Results

In this section we describe detailed results on a subset of the 22 samples, representative of the different clast assemblages, sulfide content and proportion of clast to matrix, beginning with sulfide-poor troctolite host rocks. We then consider different variants of sulfide ore breccias.

Consistency of terminology for the complex, highly heterogeneous rocks seen at Voisey's Bay and in many other mafic-hosted Ni sulfide deposits is problematic. A number of terms are in common use at Voisey's Bay that either are unique to the deposit or are used differently in other places, notably "leopard texture", and "vari-textured" (Evans-Lamswood et al., 2000). The term "leopard texture" has been used to denote a type of net-textured ore (idiomorphic silicate grains embedded in a continuous matrix of originally liquid sulfide) that contains prominent dark spots; these spots can be either small silicate xenoliths, or more commonly large single-crystal clinopyroxene or olivine oikocrysts, as discussed in detail below. We reserve the term here for where the spots are oikocrysts; the texture could also be denoted as pyroxene-poikilitic (or less commonly olivine-poikilitic) net-textured ore. The term "vari-textured" is reserved for use to describe olivine gabbros and troctolites, either as distinct rock type or constituting the matrix to breccias with externally derived clasts, and denotes rapid fluctuations in grain size from less than 1 mm to several cm on a scale of a few cm.

Results are presented in various ways in order to best reveal the critical textures. For the most part we use false-colour three-element concentration maps, whose construction is described above in the Methods section. In some cases, these images have been translated into phase maps showing individual silicate and sulfide mineral phases (e.g. Fig. 3); however, this translation produces misleading results where the grain size (particularly in the paragneiss xenoliths) is less than the 40 μm spatial resolution of the scan so we restrict it to coarse grained xenolith-poor rocks. We also use standard optical photomicrographs and backscattered electron SEM images where appropriate to illustrate particular textures at scales finer than the 40 μμm resolution of most of the XRF maps.

4.1. Sulfide-poor and sulfide-rich olivine gabbros

Olivine gabbros in the various components of the Voisey's Bay system are characteristically poikilitic. The dominant oikocryst mineral is augite. Plagioclase occurs most commonly as smaller grains ophitically enclosed within the augite; olivine forms ophitic or poikilitic grains around plagioclase in some cases, and as enclosed grains within clinopyroxene in others.

A typical sulfide-poor olivine gabbro, shown in Fig. 3, consists of randomly oriented plagioclase laths with partially interstitial oli-

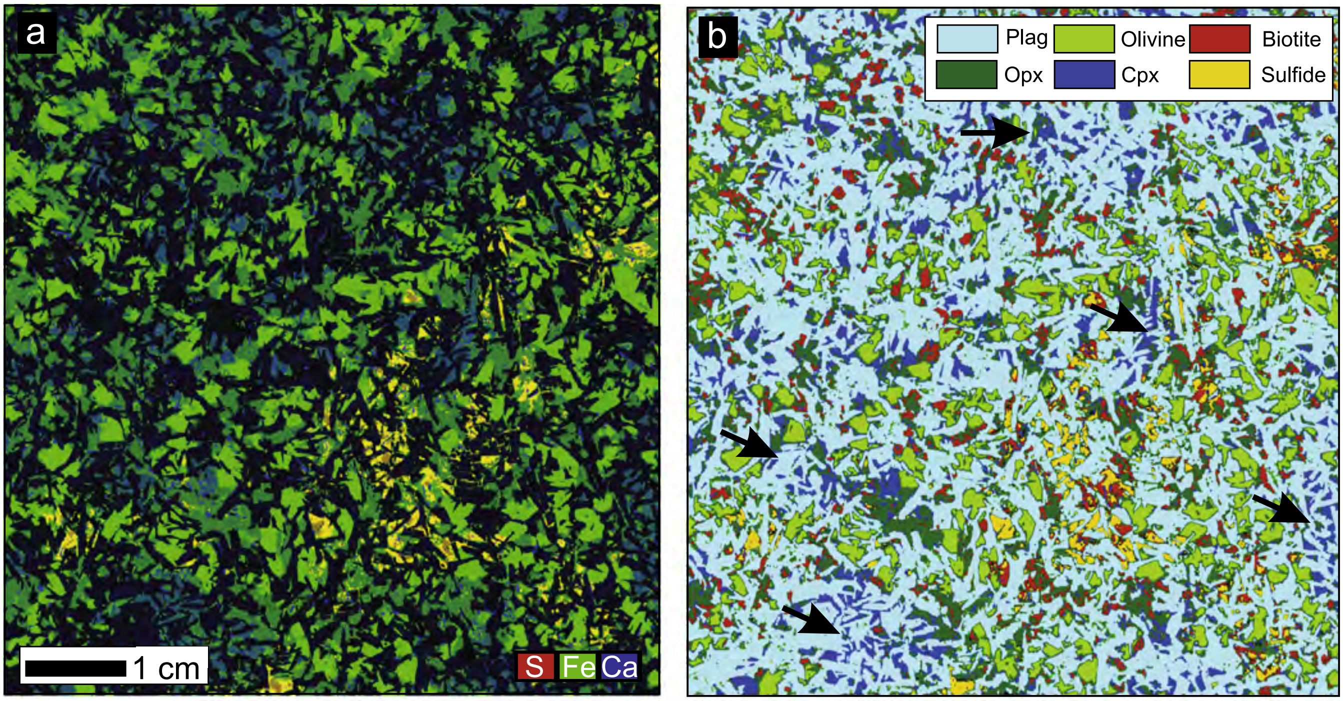

Fig. 3. (a) Tornado XRF map (S red, Fe green and Ca blue) sample ED04, transformed into (b) phase map showing distribution of plagioclase (plag), olivine, biotite, clinopyroxene (cpx), orthopyroxene (opx) and sulfide minerals (other accessory minerals are present but not shown). See Methods section for a description of how these maps are constructed. Note the characteristic non-cumulate ophitic-doleritic texture. Cpx forms oikocrysts 1–2 cm across. (For interpretation of the references to colour in this figure legend, the reader is referred to the web version of this article.)

vine in a characteristic ophitic texture, containing clinopyroxene oikocrysts typically about 1 cm across, subordinate proportions of interstitial orthopyroxene forming rims on olivine in areas outside clinopyroxene oikocrysts, and minor patches of interstitial sulfide, also restricted to areas outside clinopyroxene oikocrysts. This textural relationship is retained in more sulfide-rich olivine gabbros, which tend to sulfide-rich troctolite as the proportions of first orthopyroxene then clinopyroxene decrease as the proportion of sulfide increases. Sample ABSB-1 (Fig. 4) occupies the troctolite end of the spectrum.

Biotite and hornblende are ubiquitous components of all sulfide-bearing Voisey's Bay samples examined in this study, characteristically forming rims between plagioclase, olivine and sulfide (Fig. 4). As a general but not universal rule, biotite forms rims around plagioclase and hornblende forms rims around olivine. A zoned assemblage occurs in places where a myrmekitic intergrowth of orthopyroxene and hornblende surrounding olivine is progressively rimmed by hornblende and biotite, as illustrated in detail below. Rapid fluctuations in plagioclase and olivine grain size occur but show no correlation with the abundance of hornblende or biotite. Corroded margins of plagioclase against biotite (e.g. Fig. 4E, G) attest to the development of biotite as a replacement of plagioclase.

A common variant of disseminated to net-textured sulfide at Voisey's Bay, termed "leopard textured" ore, consists of plagioclase, olivine oikocrysts and clinopyroxene oikocrysts in a continuous sulfide matrix. The oikocrysts form prominent dark "leopard spots" (Fig. 5). A noteworthy feature of this image is the low abundance of inclusions of olivine or sulfide within the clinopyroxene oikocrysts. This is a directly analogous ore type to poikilitic net-textured ore observed in olivine-pyroxene-sulfide rocks in komatiite-hosted ores (Barnes et al., 2017), the only difference being the presence or absence of plagioclase in komatiitic sulfides.

4.2. Sulfide matrix breccias

The term "sulfide-matrix breccias" is used where sulfide forms a continuous or near continuous matrix between the clasts. A number of samples showing subtly different variations in texture and clast populations are described here, primarily on the basis of microbeam XRF images.

Sample Ov05 from the breccia zone beneath the Ovoid massive sulfide is a typical example of a clast-supported (i.e. comprising a continuous framework of touching clasts as imaged in 3D) sulfide matrix breccia (Fig. 6) showing three types of clasts: 1) peridotite, consisting of olivine orthocumulate with interstitial plagioclase, clinopyroxene, hornblende and phlogopite; 2) fine-grained troctolite to olivine gabbro; and 3) strongly banded hercynite-anorthite paragneiss with hercynite pseudomorphing corundum needles A distinctive feature of this and most of the sulfide-matrix ore breccias at Voisey's Bay is the presence of radiating plagioclase laths, developed as overgrowths on all clast types but particularly on the paragneiss clasts. The radiating plagioclase laths evidently nucleated on finer grained granular plagioclase of similar composition that developed as a rind around the hercynite-anorthite clast cores. The resulting plagioclase framework texture extends outward from the clasts into the interiors of the sulfide-rich domains (Fig. 6). Also noteworthy is the presence of biotite (red on the K-Ca-Si maps, e.g. Figs. 4g, 6b) preferentially developed on the margins of the paragneiss clasts, to a lesser extent within some of the paragneiss clasts and less abundantly at the margins of the ultramafic clasts. Note that the pentlandite grains (dark brown in Fig. 6) completely overprint the silicate texture, reflecting their late and relatively low T origin.

The ultramafic clasts in this sample are composed of fine to medium grained olivine orthocumulate with interstitial plagioclase, clinopyroxene, hornblende, biotite and green translucent

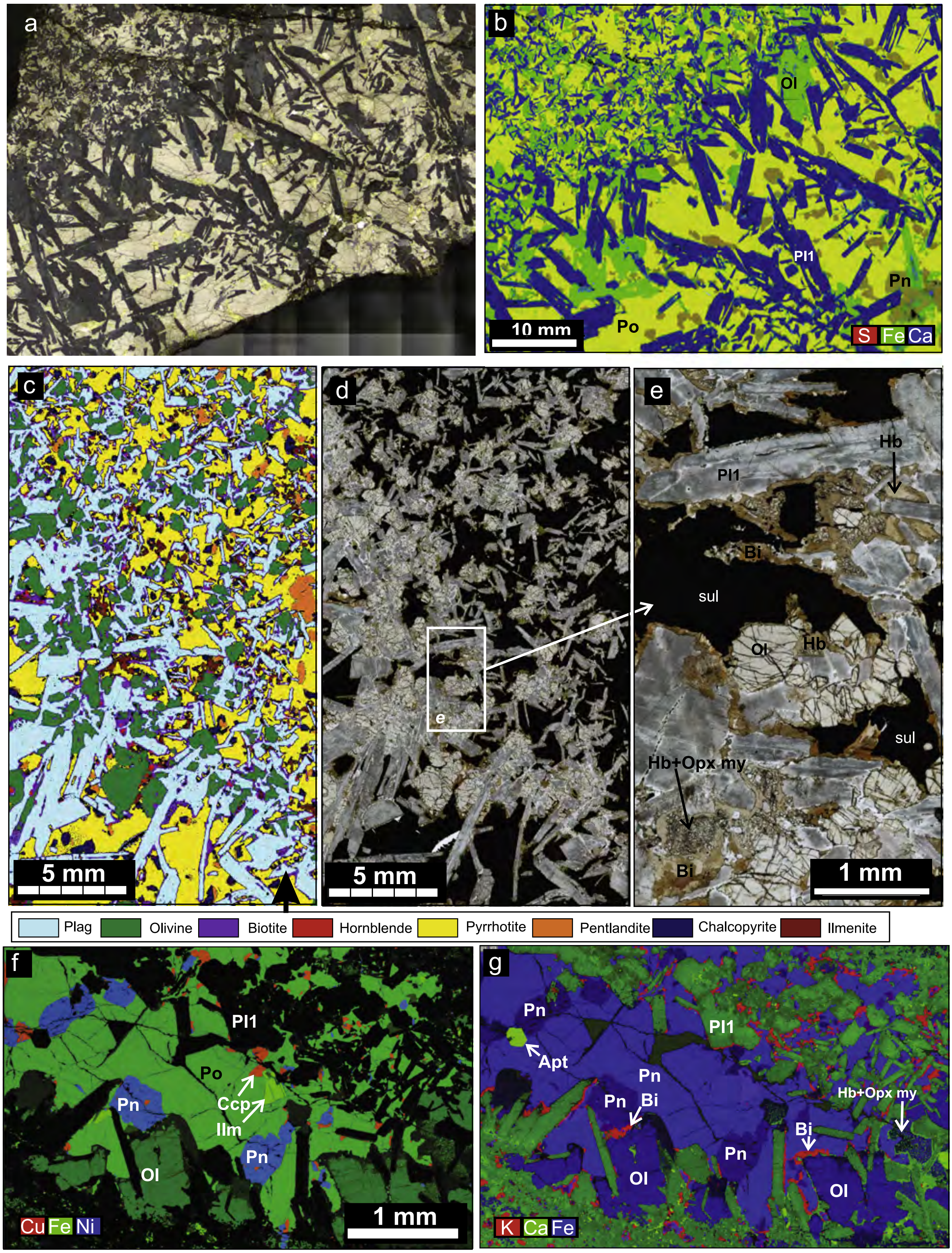

Fig. 4. Sulfide-rich vari-textured troctolite, sample Ov02. (a), Optical image of polished slab. (b), Tornado XRF element map of sample slab. Ol = olivine, Pl1 = "framework"-type plagioclase, o = pyrrhotite, Pn = pentlandite. (c-e) – images of a thin section of the same sample. (d) is transmitted light optical photomicrograph of whole thin section, (c) is a phase map generated from an XRF map of the same area: legend refers to (c). (e), transmitted light photomicrograph of detailed area in (d), Pl1 = framework plagioclase, Sul = sulfide, Hb = hornblende, Hb-Opx My = myrmekites intergrowth of hypersthene and hornblende. Bi = biotite. Note irregular embayed geometry of biotite-plagioclase contacts. (f) and (g): High-resolution (4 μm pixel) synchrotron XFM element maps showing relationship of silicate, oxide and sulfide phases. Ilm = ilmenite, Apt = apatite.

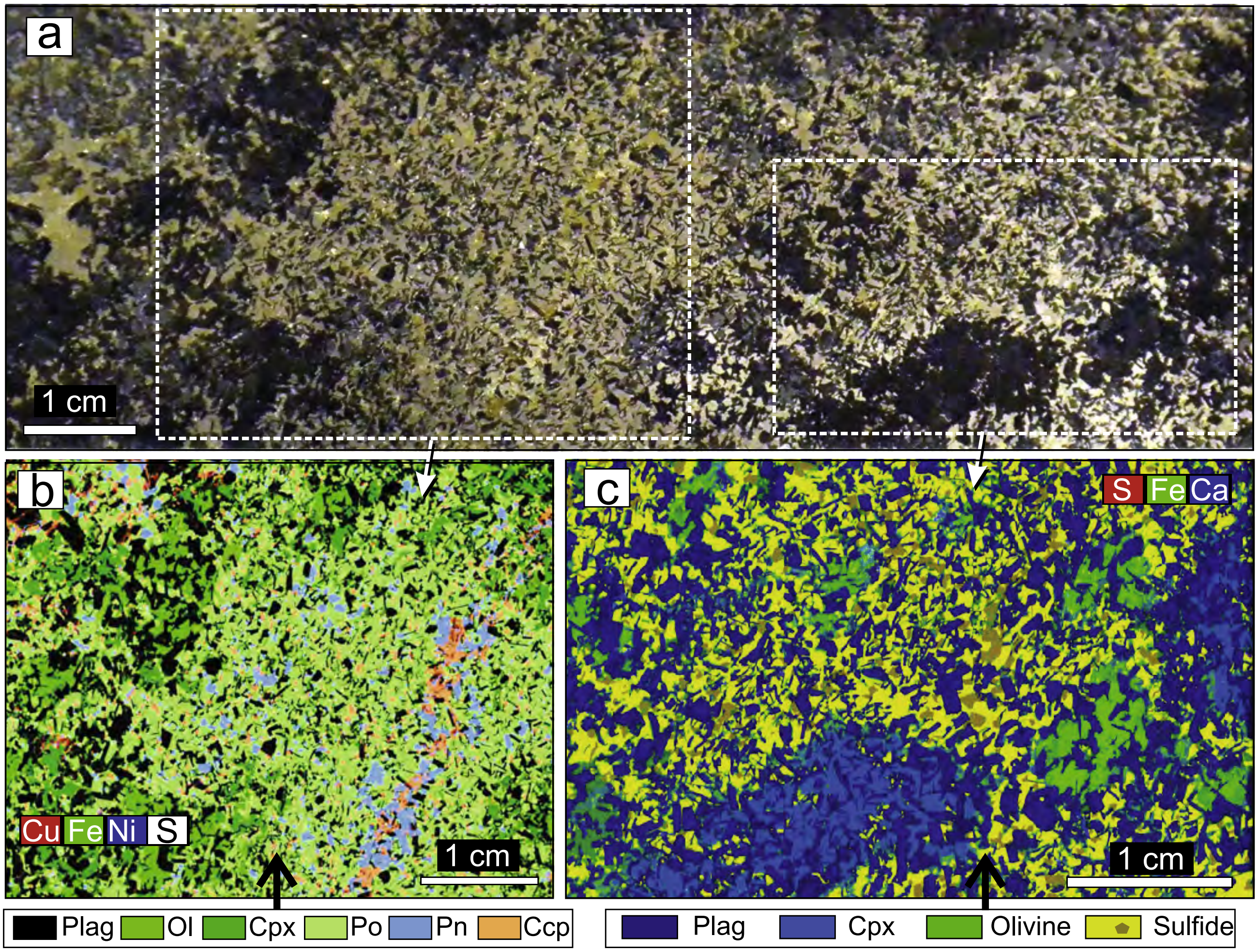

Fig. 5. "Leopard-textured" ore sample – VB95-39. Polished slab and XRF image showing large "spots" are formed by both clinopyroxene and olivine oikocrysts. Note paucity of sulfide and olivine inclusions within the cpx, and of sulfide inclusions within the olivine.

spinel (Fig. 6c,d). The matrix adjacent to these clasts comprises coarse plagioclase with interstitial space occupied by complex reaction-sequence intergrowths of clinopyroxene, rimmed by orthopyroxene, symplectic hornblende-olivine intergrowths and biotite (Fig. 6e,f).

3D tomography (Fig. 7) shows that the breccia is clast supported and indicates that the plagioclase outgrowths on the clasts form part of a continuous plagioclase framework extending throughout much of the sulfide matrix. Furthermore, the sulfide mass forms an almost completely interconnected 3D framework extending through the entire hand sample.

Sample OV02 shows very similar features to Ov05, with particularly clear development of biotite and hornblende rims on plagioclase and olivine respectively, developed at the margin of paragneiss clasts (Figs. 8 and 9). (The mica is actually mid-way between biotite and phlogopite but referred to as biotite for convenience). Photomicrographs (Fig. 8) show distinct zoning in the habit and abundance of hercynite (pseudomorphic after corundum) within the paragneiss clasts, as described by Li and Naldrett (2000). The narrow rim of plagioclase around this clast is overgrown by the idiomorphic coarse plagioclase laths that extend into the sulfide domains. These plagioclase grains are marked by very cloudy inclusion-rich cores; they commonly have narrow clear rims, which are missing where in contact with biotite (Figs. 8B, C, E, 9A). An interesting feature of this and other samples of this rock type is localized bending of plagioclase grains at impingement points of grains immersed in sulfide (Fig. 8F). Biotite rims here form along some internal plagioclase grain surfaces that appear to have formed during this deformation, and the biotite grains themselves are undeformed, with interesting implications for the timing of the biotite formation, as discussed below. Zoning in plagioclase is evident in the Ca element map obtained using high-resolution synchrotron XFM mapping (Fig. 9C). The plagioclase around the margin of the hercynite-rich paragneiss inclusion core has the highest Ca content, dropping off into the equant plagioclase rind and the lathy (PL1) outgrowths, which have homogenous unzoned cores with similar compositions to the rind grains. The laths have slightly less calcic outer zones in some grains, apparently related to alteration along fine cracks. Plagioclase tend to show irregular, corroded margins against biotite compared with planar crystal faces against sulfide, olivine and hornblende (see also Fig. 4e).

Sample ED02 from the Eastern Deeps (Fig. 10) is a sulfide-matrix breccia containing a clast of variable grain size ("varitextured") unmineralised olivine gabbro (OGb) with a narrow rim of olivine plus plagiolase extending into sulfide matrix. There is extensive development of biotite at the contact between sulfide and banded paragneiss clasts, and a very sharp boundary between a hercynite–rich paragneiss clast core and its plagioclase-rich rim (right centre). Fig. 10C shows development of sub-skeletal ilmenite and trace apatite (Apt) around margins of sulfide in areas devoid of biotite.

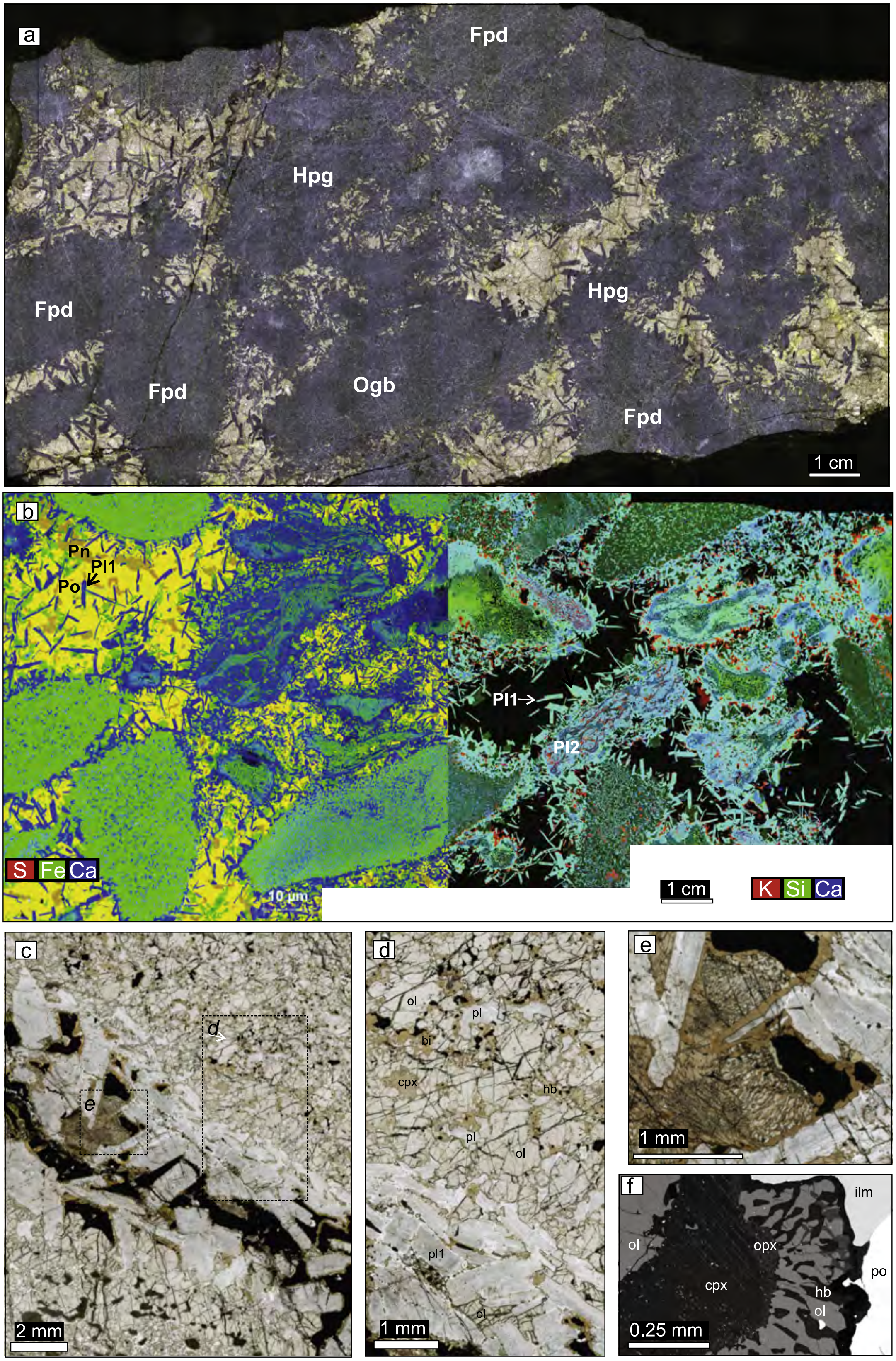

Fig. 6. Polished slab (a) and Tornado XRF element concentration maps (b) of sample Ov05. Clast supported sulfide matrix breccia showing clasts of felspathic peridotite (Fpd), consisting of olivine orthocumulate with interstitial plagioclase and clinopyroxene; fine-grained troctolite to olivine gabbro (Ogb); and strongly banded hercynite-anorthite paragneiss (Hpg). Plagioclase laths (Pl1) form outgrowths on clasts, extending into sulfide-rich domains. Pl2 denotes the fine-grained more anorthitic plagioclase developed within the paragneiss clasts. Banding within the paragneiss clasts (b, top centre left) mainly reflects varying extent of hercynite replacement of corundum. Biotite (red) is developed primarily around the margins of clasts. (c) to (e), transmitted light photomicrographs showing details of ultramafic clasts and their margins. Note plagioclase (pl), clinopyroxene, hornblende (hb) and minor biotite as interstitial phases within the clast. (e) cpx rimmed by symplectic hornblende-olivine intergrowth adjacent to sulfide at the edge of the clast. (f) backscattered electron micrograph, same field of view as (e).

Please cite this article in press as: Barnes, S.J., et al. Textural development in sulfide-matrix ore breccias in the Voisey's Bay Ni-Cu-Co deposit, Labrador, Canada. Ore Geology Reviews (2017), http://dx.doi.org/10.1016/j.oregeorev.2017.03.019

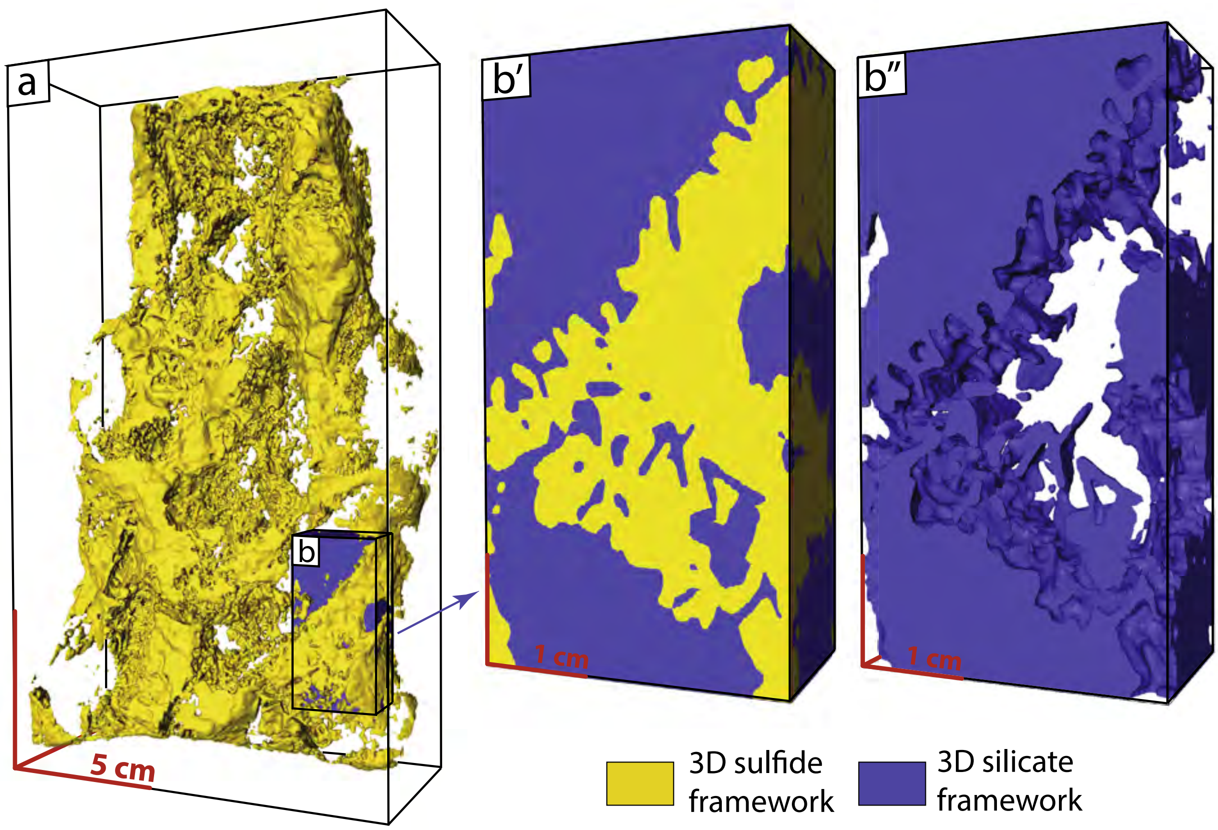

Fig. 7. 3D X-ray tomographic image of sample Ov05 showing 3D distribution and connectivity of sulfides, and morphology of the plagioclase framework. Animated version can be viewed at https://www.youtube.com/watch?v=hUGN9Lvt-08.

Sample ED10 (Fig. 11) from the Eastern Deeps basal breccia sequence is another clast supported sulfide matrix breccia (the clast supported character is confirmed in 3D) with variably hercynite-bearing paragneiss clasts and clasts of mainly unmineralised olivine gabbro with characteristic plagioclase lath framework and interstitial olivine. This sample is significant in containing a relatively high proportion of silicate-sulfide matrix, which consists of "leopard-textured" mineralised troctolite (enlarged area shown as Tornado XFM map of S-Fe-Ca in Fig. 11f) with large clinopyroxene oikocrysts. The similarity of this texture to that of the clast-poor mineralised olivine gabbros and troctolites is noteworthy and is discussed in detail below. The texture of the oikocrysts is also noteworthy in that (1) they are largely devoid of sulfide and olivine inclusions, and (2) that they enclose plagioclase grains showing an identical framework of laths as that seen away from the oikocrysts in the sulfide-rich areas (e.g. Fig. 11F).

4.3. Sulfide-poor silicate-matrix breccias

Sulfide-poor breccias vary in a number of features: the proportion and make-up of the xenolith population, the proportion of sulfide to olivine gabbro in the inter-clast matrix, and the proportions of plagioclase and olivine in the sulfide domains. Sample ED-PL-Bx1 from the Eastern Deeps (Fig. 12) is a good example of a variant with very clean, silicate-free sulfide domains, associated with very irregular-shaped paragneiss xenoliths showing very well-developed milky plagioclase rinds. In this sample as in others olivine gabbro is present both as endogenous clasts and as the inter-clast matrix.

The final sample illustrated in detail here, Ov06, (Fig. 13, Fig. 14) is a xenolith-rich, sulfide-poor, clast-supported intrusion breccia with extensively reacted paragneiss clasts with corundum-plagioclase cores and hercynite-plagioclase rims (Fig. 13 a-d). The distinctive feature of this sample is the continuous network matrix of variable sulfidic poikilitic olivine gabbro. The anorthositic clasts show extensive development of less calcic plagioclase rims grading indistinctly into the olivine gabbro matrix. The olivine gabbro matrix shows a number of distinctive features developed in the interstices of the plagioclase framework including finely intergrown olivine and sulfide (Fig. 13 d,f) and pockets of symplectite plagioclase-orthopyroxene intergrowth passing into hornblende, biotite, ilmenite and apatite (Fig. 13 e, g). These are interpreted as pockets of eutectic residual melt. Significantly, despite the low modal abundance of sulfide (less than 10%in this sample), it forms an extensively interconnected network throughout the sample.

This rock type is seen as an equivalent of the paragneiss-rich sulfide matrix breccia but with much less sulfide. The textures within the poikilitic olivine gabbro matrix show wide variation in grain size, corresponding to the vari-textured inclusion-free gabbros elsewhere in the complex, but have essentially identical textures to the olivine gabbro components of the other samples studied.

5. Discussion

5.1. Summary of critical features

A number of critical features have been identified within the spectrum of lithologies imaged here. These provide some key constraints on genetic processes.

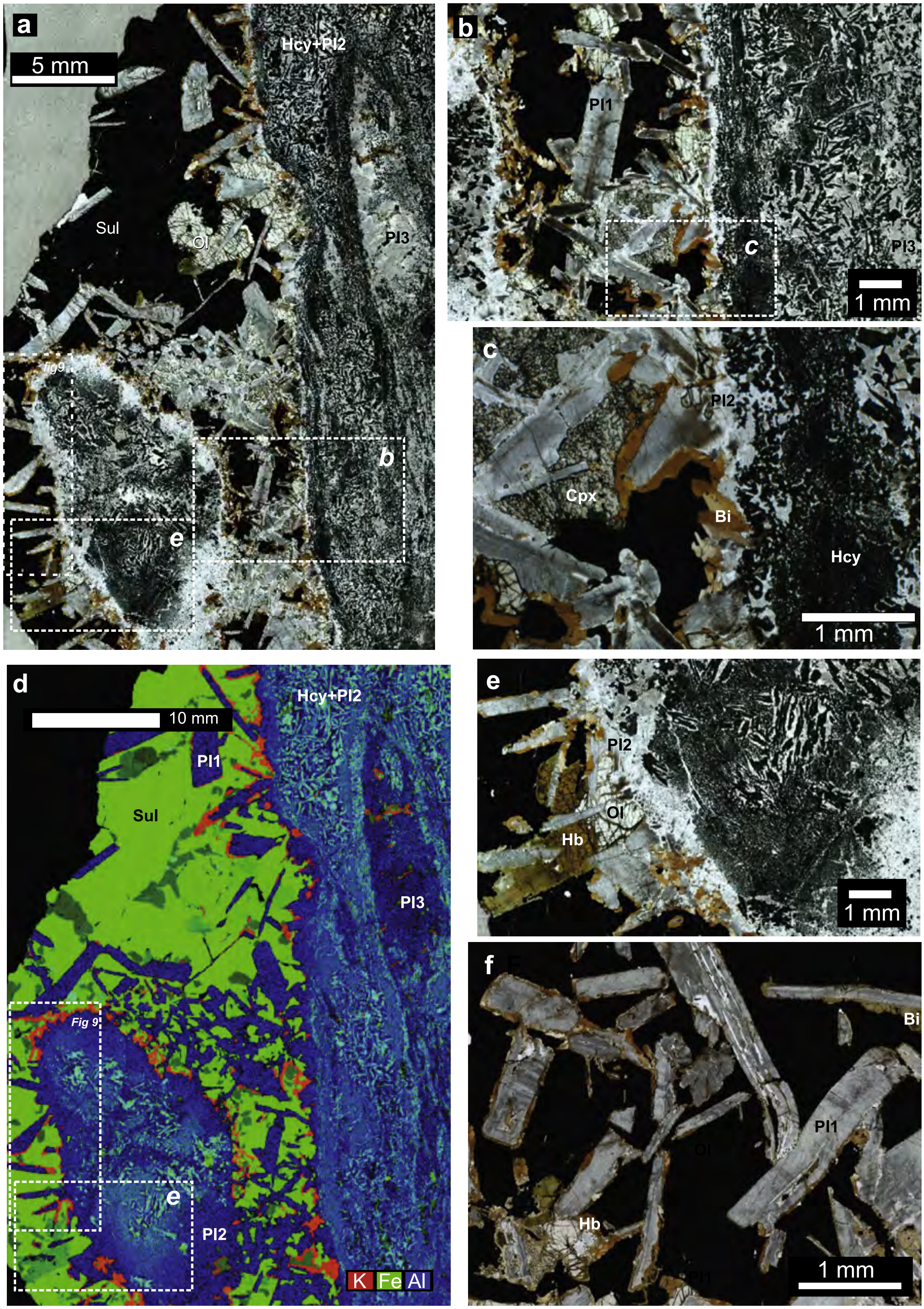

Fig. 8. Sample Ov02, polished thin section 1A, transmitted light, uncrossed polars. (a) Photomicrograph of whole thin section, (d) Tornado XRF map of same area; biotite shows in orange. Box labelled "Fig 9" indicates area of synchrotron element maps in Fig. 9. Sul = sulfide, Ol = olivine, Cpx = clinoopyroxene, Hcy = hercynite, pseudomorphic after corundum, Pl3 = anorthite plagioclase from core of paragneiss xenoliths. Pl2 = labradorite plagioclase rims, PL1 = labradorite plagioclase framework-forming laths. Bi = biotite, Hb = hornblende. Note the strong concentric modal zoning of the paragneiss clasts, with alternating bands of variable abundance of coarse and fine hercynite intergrown with Ca-rich plag (Pl3). Xenoliths all have an outer rim of pure plagioclase Pl2, overgrown by less calcic radiating plagioclase laths (Pl1) with interstitial olivine and clinopyroxene. Biotite characteristically forms rinds between Pl1 and sulfide; hornblende forms rinds between olivine and sulfide in proximity to plagioclase. Pl1 plagioclase has distinctive cloudy cores and clear rims but lacks compositional zoning. (f): bending of plagioclase at impingement points of grains immersed in sulfide. Note that biotite forms along some plagioclase grain surfaces formed during this deformation.

Please cite this article in press as: Barnes, S.J., et al. Textural development in sulfide-matrix ore breccias in the Voisey's Bay Ni-Cu-Co deposit, Labrador, Canada. Ore Geology Reviews (2017), http://dx.doi.org/10.1016/j.oregeorev.2017.03.019

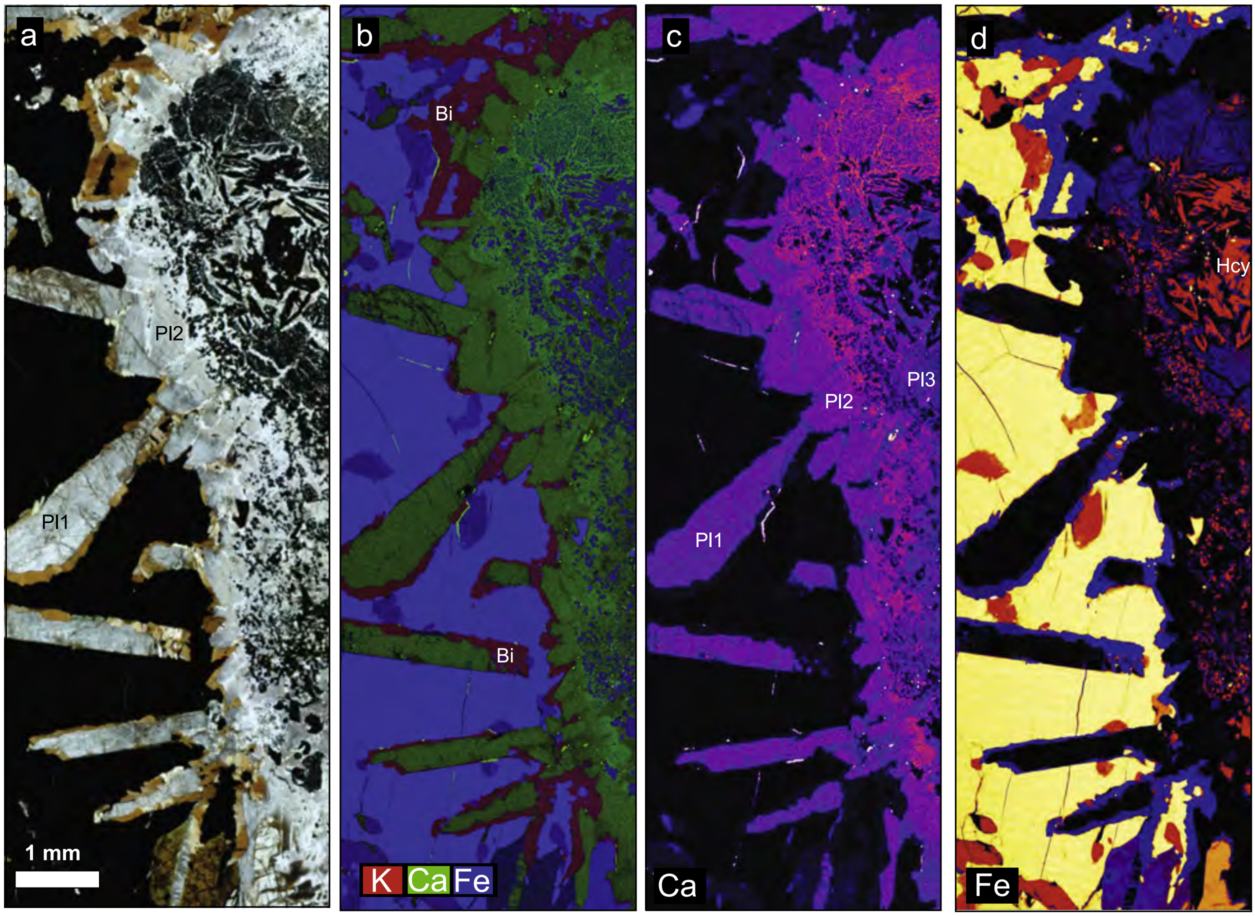

Fig. 9. High resolution synchrotron-XFM chemical composition maps for area labelled "Fig. 9" in Fig 8, sample Ov02, with the same abbreviations for phase labels. (a) Transmitted light, uncrossed polars. (b), three element map with K red, Ca green, Fe blue. (c) and (d) respectively, single element maps for Ca and Fe with element abundance shown in colour spectrum from black (low) through blue and red to yellow (high). Note the sharp change from Ca-rich Pl2 plagioclase intergrown with hercynite to less calcic, normally zoned Pl1 grains. Also note apparently replacive relationship of biotite surrounding corroded Pl1 plagioclase. (For interpretation of the references to colour in this figure legend, the reader is referred to the web version of this article.)

1. Plagioclase laths (designated Pl1 in the images) form 3D frameworks with essentially identical textures regardless of whether enclosed in clinopyroxene oikocrysts, in sulfide-rich net-textured troctolite, or in sulfide-poor olivine gabbro domains forming the matrix to sulfide-rich and sulfide poor breccias. To put it another way (Fig. 15) the textural framework of the olivine gabbro is independent of the sulfide content and the proportion of clasts. The geometry of the framework is independent of grain size – coarse and fine grained domains have the same texture, probably reflecting variable diffusion rate (water content) of the matrix during crystallisation. The only consistent difference between plagioclase morphologies in sulfide-rich and sulfide-poor domains is that the larger grains in sulfide-rich domains are commonly slightly bent (e.g. Fig 15. d), implying a small degree of deformation and compaction.
2. The proportion of pyroxene decreases with increasing sulfide content, such that poikilitic clinopyroxene is low or absent in the most sulfide-rich samples (e.g. Fig. 4).
3. All clast types, hercynite-bearing paragneiss and igneous, have similar and typically sharp overgrowth of olivine gabbro with framework plagioclase. This implies that the olivine gabbro represents the crystallisation product of the liquid matrix. There is little evidence of *in situ* interaction between the clasts and the olivine gabbro matrix.
4. Paragneiss clasts are devoid of sulfide. All of the sulfide is intergrown with the plag + olivine+/-cpx olivine gabbro/troctolite assemblage, either within troctolite clasts or within the matrix. This is significant in that the Tasiuyak gneiss formation from which these clasts are generally agreed to have been derived contains abundant sulfides.
5. Clast types comprise endogenously-derived olivine cumulates, olivine-plagioclase cumulates, olivine gabbros with ophitic textures representing liquids, and country rock paragneisses that have highly refractory restite compositions. The anorthositic rind around the hercynite-bearing paragneiss clasts is either a reaction product between clast and silicate melt as inferred by Li and Naldrett (2000), or more likely a zone from which partial melt has been completely extracted leaving a monomineralic residue.
6. Sulfide in all samples, down to modal abundances less than 10 modal percent sulfide, forms fully interconnected three dimensional networks at hand-sample scale. In the more sulfide breccias, e.g. the Eastern Deeps samples, this network probably extends over several metres.
7. All of the sulfide-rich breccias imaged in this study are clast-supported, including those with the highest proportion of sulfide matrix; this is not always apparent from 2D sections, but is revealed by the 3D tomography.
8. Biotite-phlogopite is developed almost ubiquitously as replacement rims between plagioclase and sulfide, but tends to be more abundant around the paragneiss inclusions, in preference to the ultramafic inclusions. Hornblende and hornblende-orthopyroxene symplectite forms rims between olivine and sulfide.

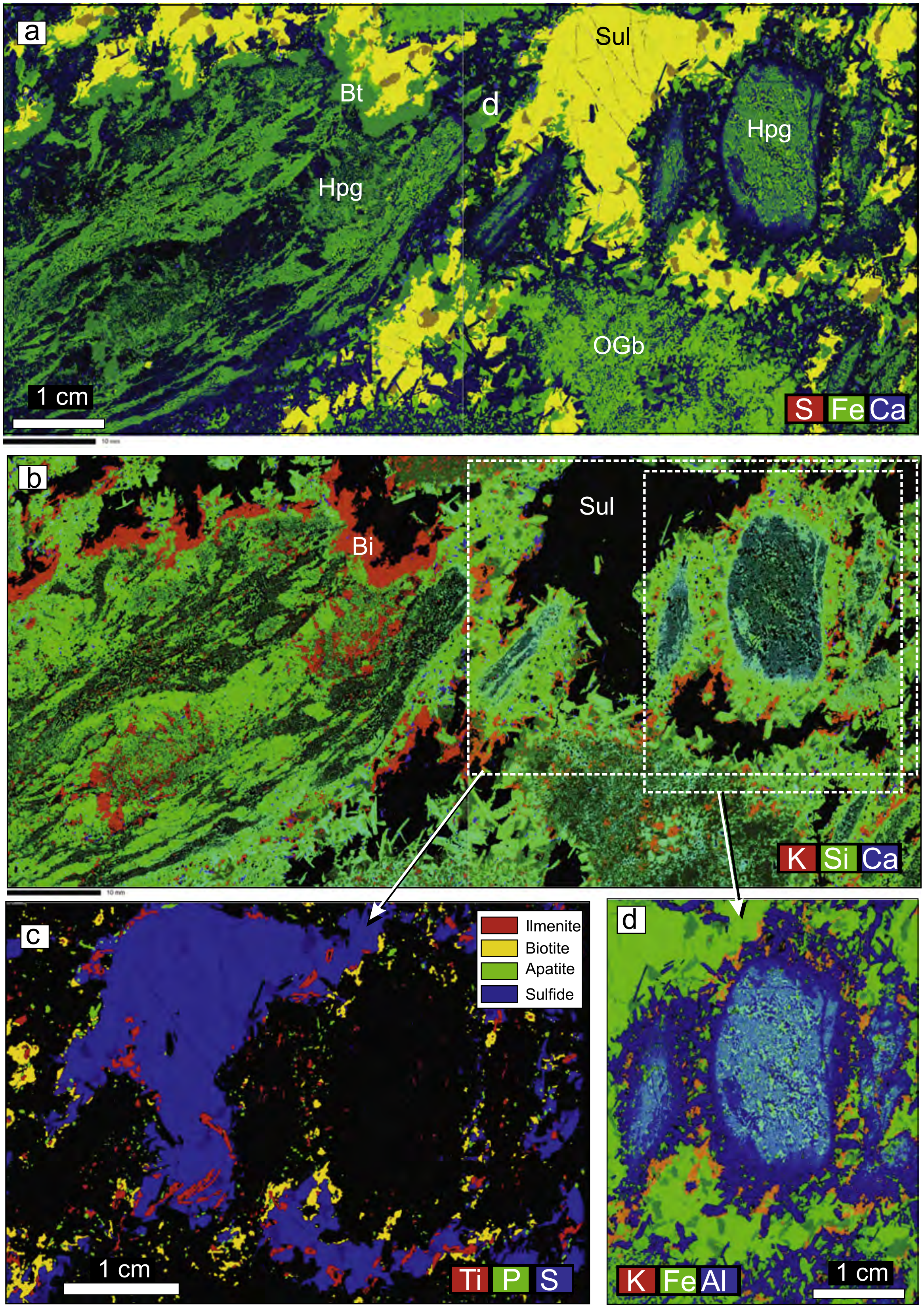

Fig. 10. Sample ED02 Tornado XRF maps. S-Fe-Ca (a), K-Si-Ca (b), Ti-P-S (c) and K-Fe-Al (d). Sulfide-matrix breccia containing banded and zoned clasts of hercynite-rich paragneiss, sulfide domains silicate-poor with silicate-poor interiors, and a clast of variable grain size ("vari-textured") unmineralised olivine gabbro (OGb), containing minor biotite, with narrow rim of olivine plus Pl1 plagiolase extending into sulfide matrix. (b), K-Si-Ca XRF map showing extensive development of biotite (Bi -orange) at contact between sulfide and banded HPg clast, and sharp boundary between hercynite–rich paragneiss clast core and Pl2 plagioclase-rich rim (right centre). (c) Shows development of sub-skeletal ilmenite and trace apatite (Apt) around margins of sulfide in areas devoid of biotite. Note the lack of a close spatial association between ilmenite, apatite and biotite. Biotite – orange in (d) – is closely associated with the plagioclase lath overgrowths on the paragneiss clasts but absent from the interiors of these clasts. (For interpretation of the references to colour in this figure legend, the reader is referred to the web version of this article.)

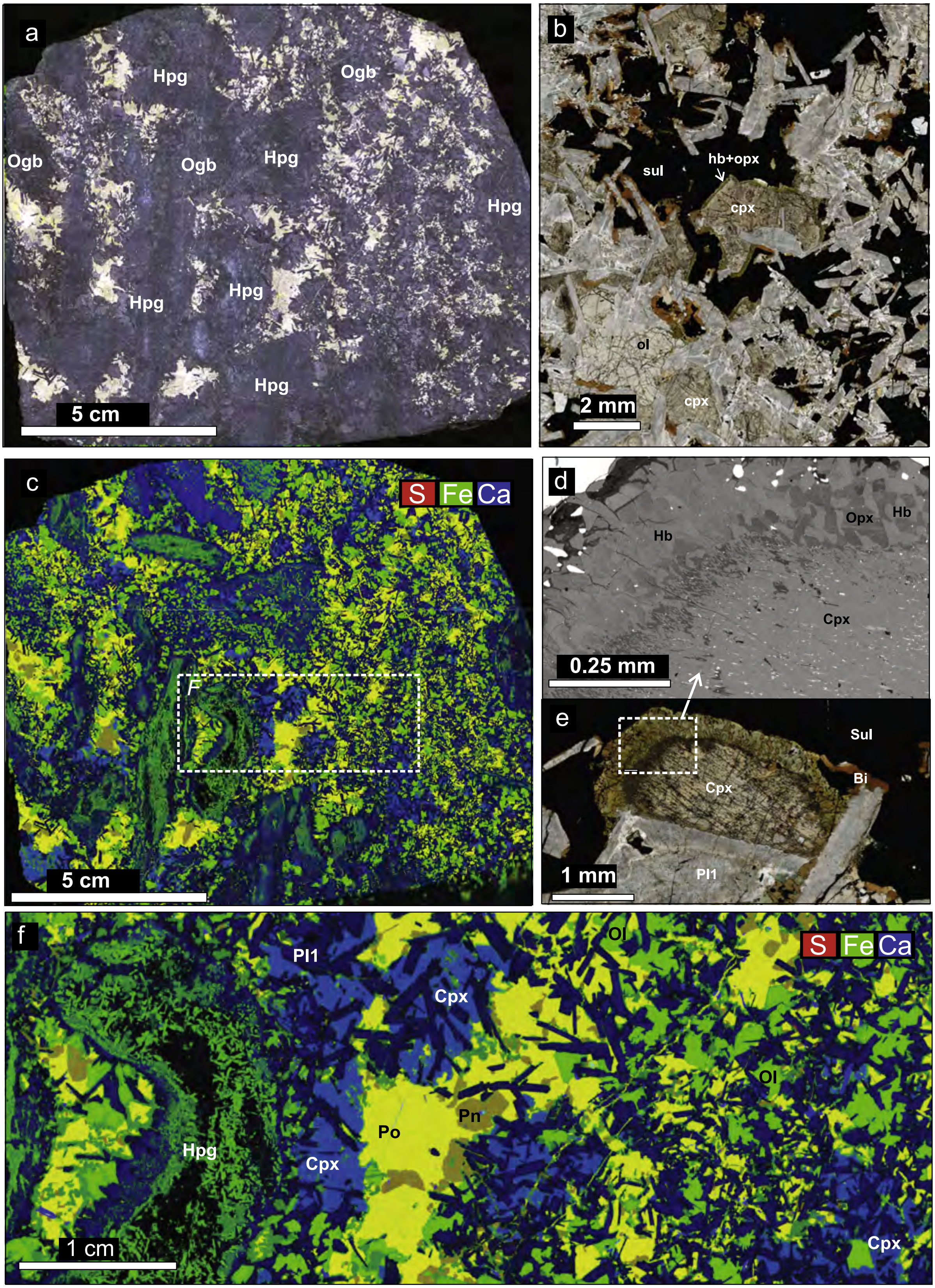

Fig. 11. Sample ED10. Clast-supported breccia with variably hercynite-bearing paragneiss clasts and clasts of mainly unmineralised olivine gabbro with characteristic plagioclase lath framework and interstitial olivine, having very similar texture to the sulfide-rich, "leopard – textured" olivine gabbro matrix. (a), optical image of slab. (b) Transmitted light photomicrograph of a section cut from the back of this slab, showing plagioclase (Pl1) framework within troctolite (lower left) and sulfide (upper right), clinopyroxene with rims of hornblende (Hb) plus othopyroxene (Opx); (c) Tornado XRF map (S-Fe-Ca) of same field of view as (a); (d) and (e) respectively, backscattered SEM and transmitted light micrograph of Cpx with Hb + Opx myrmekites rim against sulfide; (f), enlarged detail of XRF map showing "leopard spots" formed by 1–2 cm clinopyroxene (Cpx) oikocrysts enclosing plagioclase lath framework, Po = pyrrhotite, Pn = pentlandite.

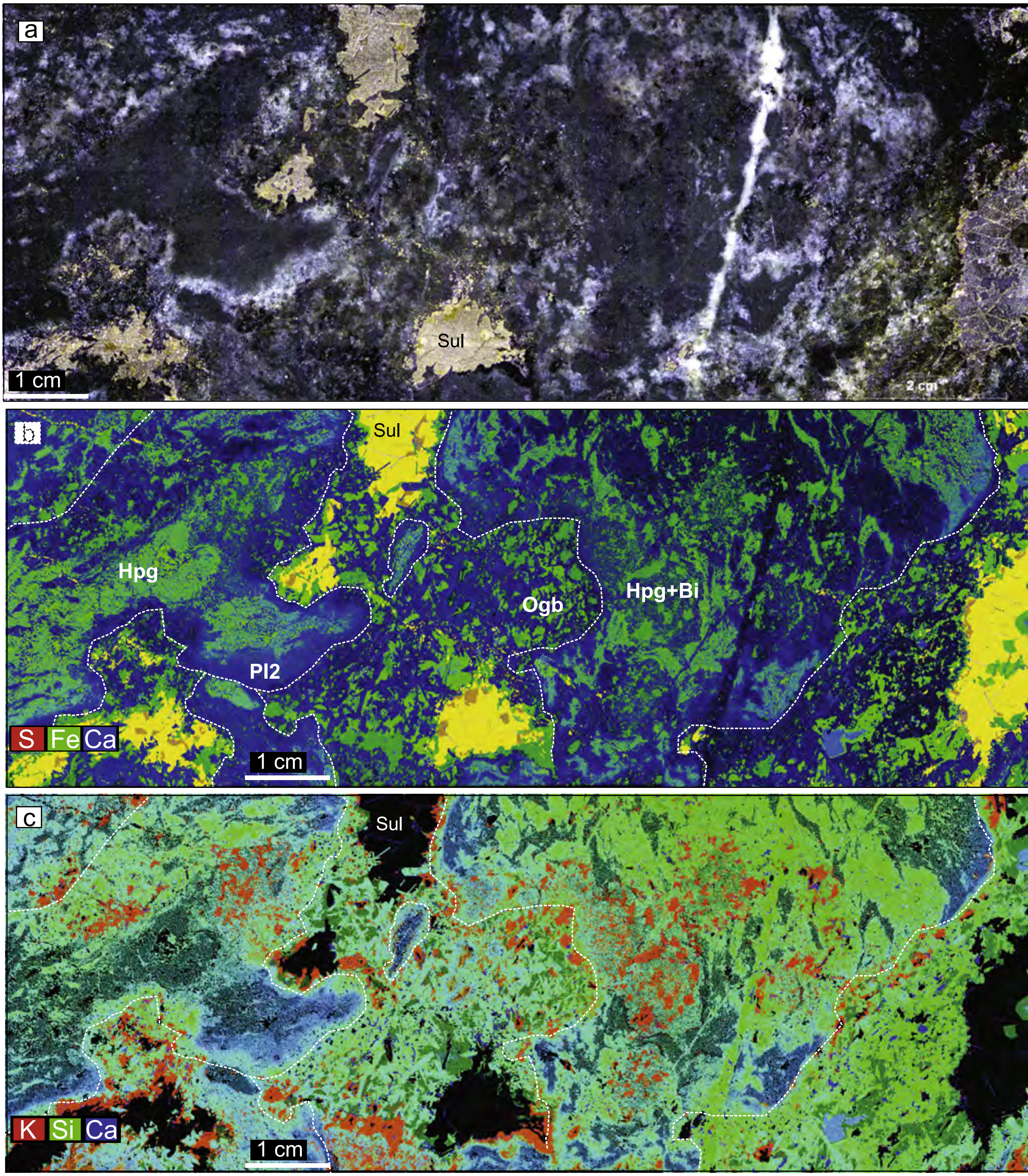

Fig. 12. Sulfide-poor breccia sample ED03 with high proportion of "soft-walled" highly irregular paragneiss clasts. (a) Optical image; note "milky" plagioclase (P2) rims on the hercynite paragneiss (Hpg) clasts; (b) Tornado XRF map showing sulfide patches within olivine gabbro (Ogb) matrix; boundaries between clasts and olivine gabbro matrix are highlighted. (c) Same field of view, Tornado XRF map with K in red highlighting the distribution of biotite (Bi, orange) around sulfide margins, within portions of the paragneiss clasts and within the olivine gabbro matrix. (For interpretation of the references to colour in this figure legend, the reader is referred to the web version of this article.)

5.2. Sulfide liquid percolation model

Barnes et al. (2017) have applied similar imaging techniques to those employed here to develop a model for the spectrum of disseminated to net-textured sulfide mineralization types in a wide variety of magmatic sulfide ores. These textures are driven largely by the gravitational tendency of sulfide liquid to migrate through permeable crystal mushes, displacing and in some cases re-melting silicates to form a melt that migrates back upwards in a counter-flow. This process is driven by the complex interplay of

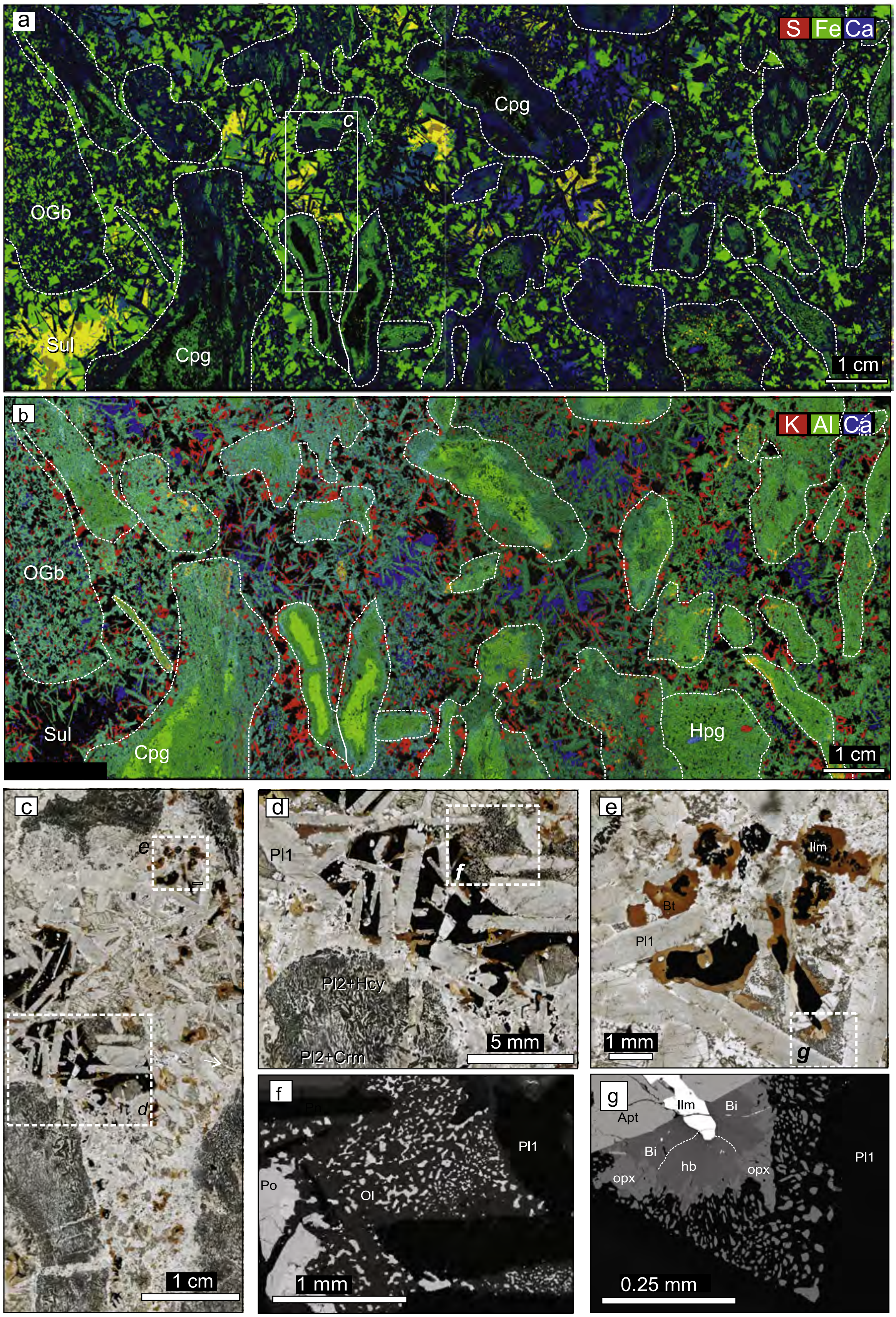

Fig. 13. Sample Ov06 XRF maps. Sulfide-poor breccia with network of weakly mineralised, variable grain size olivine gabbro interstitial to mixture of corundum and hercynite paragneiss (Cpg, Hpg) and sulfide-free olivine gabbro (OGb) clasts. (a, b), Tornado XRF maps with clast boundaries outlined in (b). c,d,e: transmitted plane polarized light optical photomicrographs, abbreviations as above, Crm = corundum. F, SEM backscattered electron image showing fine intergrowth of olivine and sulfide in interstices between plagioclase grains. G, fractionated interstitial silicate melt pocket in interstices between plagioclase grains, showing inward development of plagioclase-opx myrmekites, hornblende, biotite, ilmenite and apatite in pocket of fractionating trapped liquid.

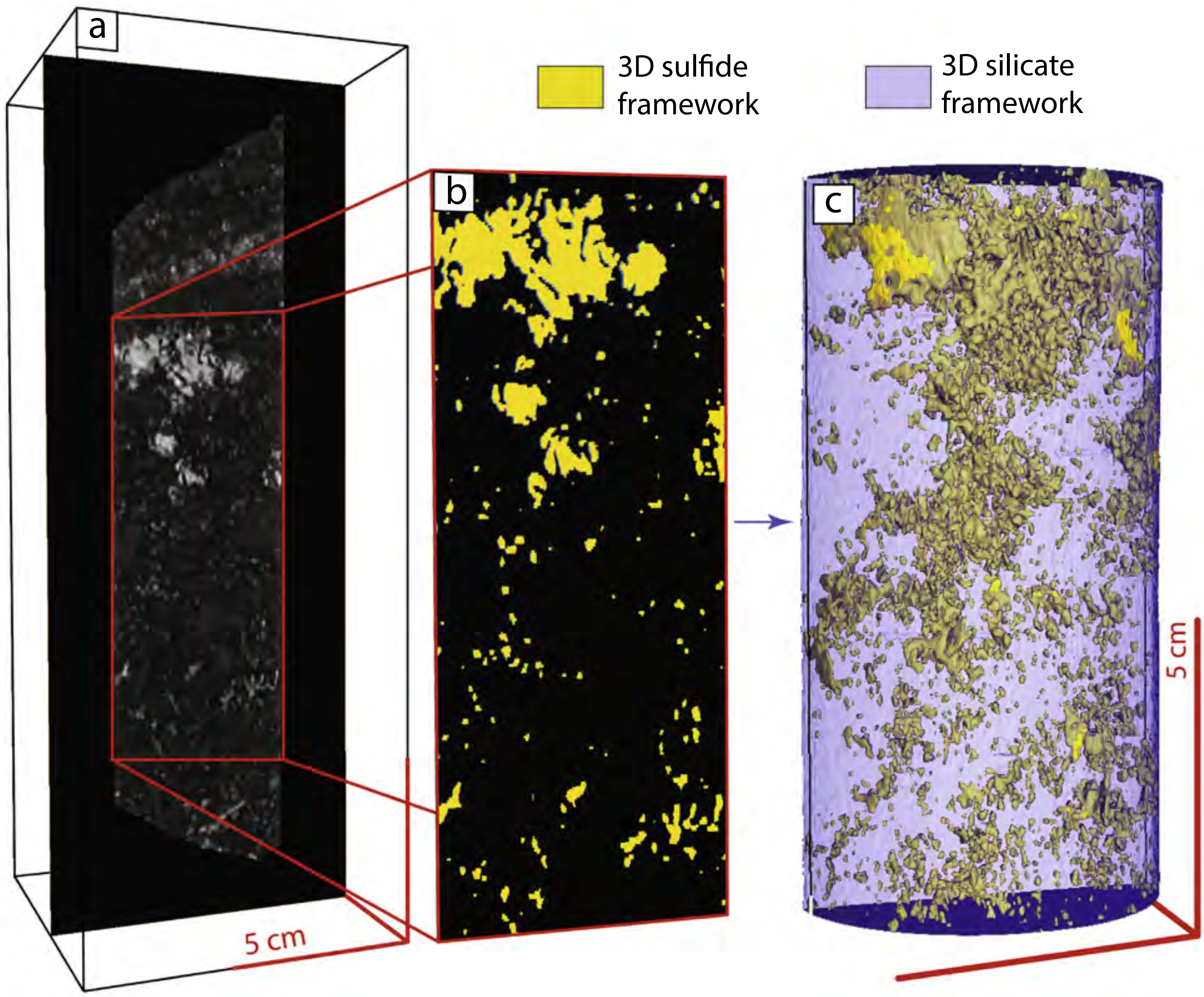

Fig. 14. Sample Ov06. 3D X-ray tomographic image showing 3D distribution and connectivity of sulfides. (a), greyscale slice through model, (b), same slice with sulfide highlighted in yellow, (c), full volume render of whole sample with silicates transparent, showing interconnectivity of the sulfide framework (yellow). (For interpretation of the references to colour in this figure legend, the reader is referred to the web version of this article.)

competitive wetting of silicates by silicate and sulfide melt and by the balance between capillary and gravitational buoyancy forces (Chung and Mungall, 2009). This gives rise to a spectrum from globular to interstitial disseminated ores leading into patchy and continuous net textured ores, in some cases with "leopard textures" defined by the presence of pre-migration pyroxene oikocrysts. A spectacular and extreme example of such textures is the development of interspinifex ore in komatiitic ore deposits, where downward percolating sulfide liquid melts and displaces silicate melt from the space in between frameworks of dendritic "spinifex" olivine crystals (Groves et al., 1986; Barnes et al., 2016a).

We propose a closely analogous model for the textural spectrum observed in the Voisey's Bay disseminated, net-textured and sulfide-matrix breccia ores described here (Fig. 16). The critical observation here is that the scale of connectivity of the sulfide networks is at least several times the characteristic particle size; this is the necessary condition for runaway intergranular percolation of sulfide liquid in the presence of co-existing silicate liquid (Chung and Mungall, 2009).

The first stage of the model postulates formation of a sulfide-poor intrusion breccia, containing a mixture of ultramafic, mafic and paragneiss clasts within a matrix of hydrous mafic liquid having the composition of the poikilitic olivine gabbro (Fig. 16a). The paragneiss clasts have already undergone extensive extraction of partial melt and reaction with assimilating magma to generate their characteristic highly refractory mineralogy of hercynite and anorthite plagioclase and rims of nearly pure anorthosite. This melting must have taken place before emplacement, to account for the evident lack of in situ contamination of the olivine gabbro matrix to the breccias. The first stage of solidification of the matrix melt involves nucleation and growth of plagioclase laths around the anorthosite rims of the clasts (Fig. 16b). Continuing growth of this plagioclase, simultaneously with crystallisation of olivine and rapid growth of clinopyroxene, gives rise to the characteristic ophitic to poikilitic textures of the interstitial olivine gabbro melt component (Fig. 16c). Concurrent with this process of matrix crystallisation, immiscible sulfide liquid percolates downward through the pore space of the breccia, driven by the relative buoyancy of the silicate liquid against the much denser and less viscous sulfide melt. As described by Barnes et al. (2017), the process is self-reinforcing as the height of interconnected sulfide liquid networks grows by coalescence within the pore space, increasing the driving pressure to overcome the opposing capillary force (Chung and Mungall, 2009). Simultaneous downward percolation of sulfide liquid with an upward counter-flow of silicate liquid results in progressive displacement of silicate melt from the pore space between the clasts and interstitial to the already established plagioclase framework. The process is exactly analogous to that of for-

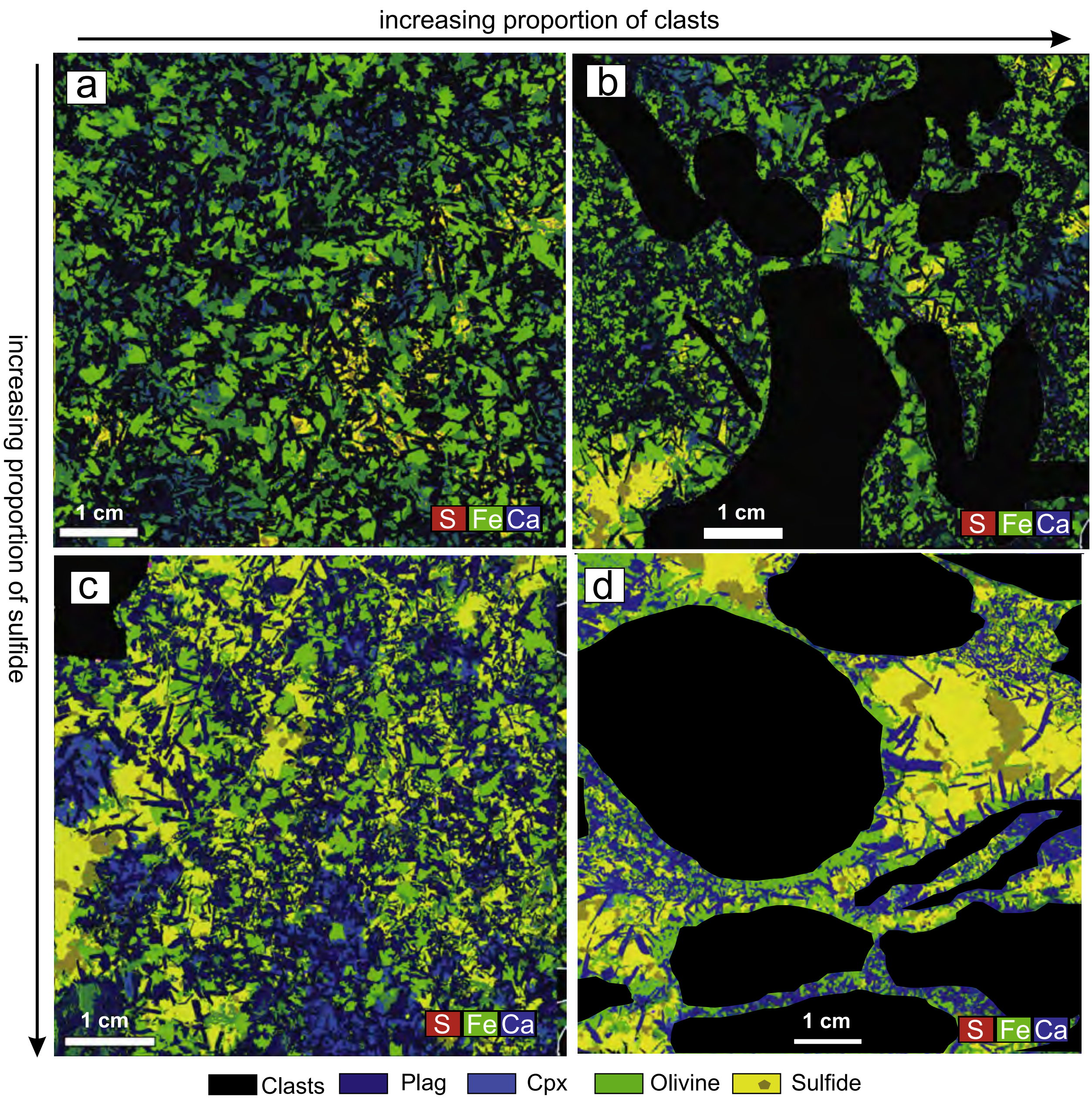

Fig. 15. Summary of textures of olivine gabbro or troctolite, in relation to the independent variables of sulfide content (increasing top to bottom row) and proportion of clasts in the breccias (increasing left to right). Clasts are deliberately shown in black to emphasize the textures in the sulfide-silicate matrix. All images shown as Tornado XRF maps at similar scale with same element combination of S red, Fe green and Ca blue (and hence same correspondence of colours to phases) as in previous images. (a), sample ED04 (Fig. 3), (b), Ov06 (Fig 13); (c), ED10 (Fig 11), (d), Ov03 (not shown elsewhere). Note the disappearance of clinopyroxene in the most sulfide rich sample (d). (For interpretation of the references to colour in this figure legend, the reader is referred to the web version of this article.)

mation of interspinifex ores and patchy net-textured ores (Barnes et al., 2017). The hydrous nature of the silicate melt keeps the residual liquid molten over much of the melting range of the sulfide melt (Barnes et al., 2016b). Vestiges of the residual silicate melt are retained as small pockets of accessory low-T phases as noted in several of the detailed descriptions. However, in many cases the residual silicate assemblage consists only of olivine and plagioclase, and in small domains only plagioclase, albeit with replacement overgrowths of biotite discussed further below. This can be explained in terms of the timing of sulfide infiltration. Infiltration during the early stages of solidification of the silicate melt component gave rise to inclusion-poor sulfide domains such as those developed in sample ED02 (Fig. 10). Later stage infiltration, after crystallisation of the plagioclase framework with poikilitic olivine and clinopyroxene, displaces a smaller proportion of residual silicate to form "leopard textures" as in sample ED10 (Fig. 11), and can result in late-stage fine intergrowths of sulfide with olivine, hornblende and biotite (e.g. Fig. 13 e,f,g). More problematic is the origin of sulfide-rich troctolite assemblages with no clinopyroxene, as in the sulfide-rich troctolite ore texture shown in Fig. 4. This could be due to timing of infiltration before the clinopyroxene has crystallised. However, formation of oikocrysts at an early, essentially cumulus stage is indicated by the absence of olivine inclusions within the clinopyroxene. Rather than forming by sequential growth as is the conventional interpretation of poikilitic textures, these relationships are better explained by simultaneous

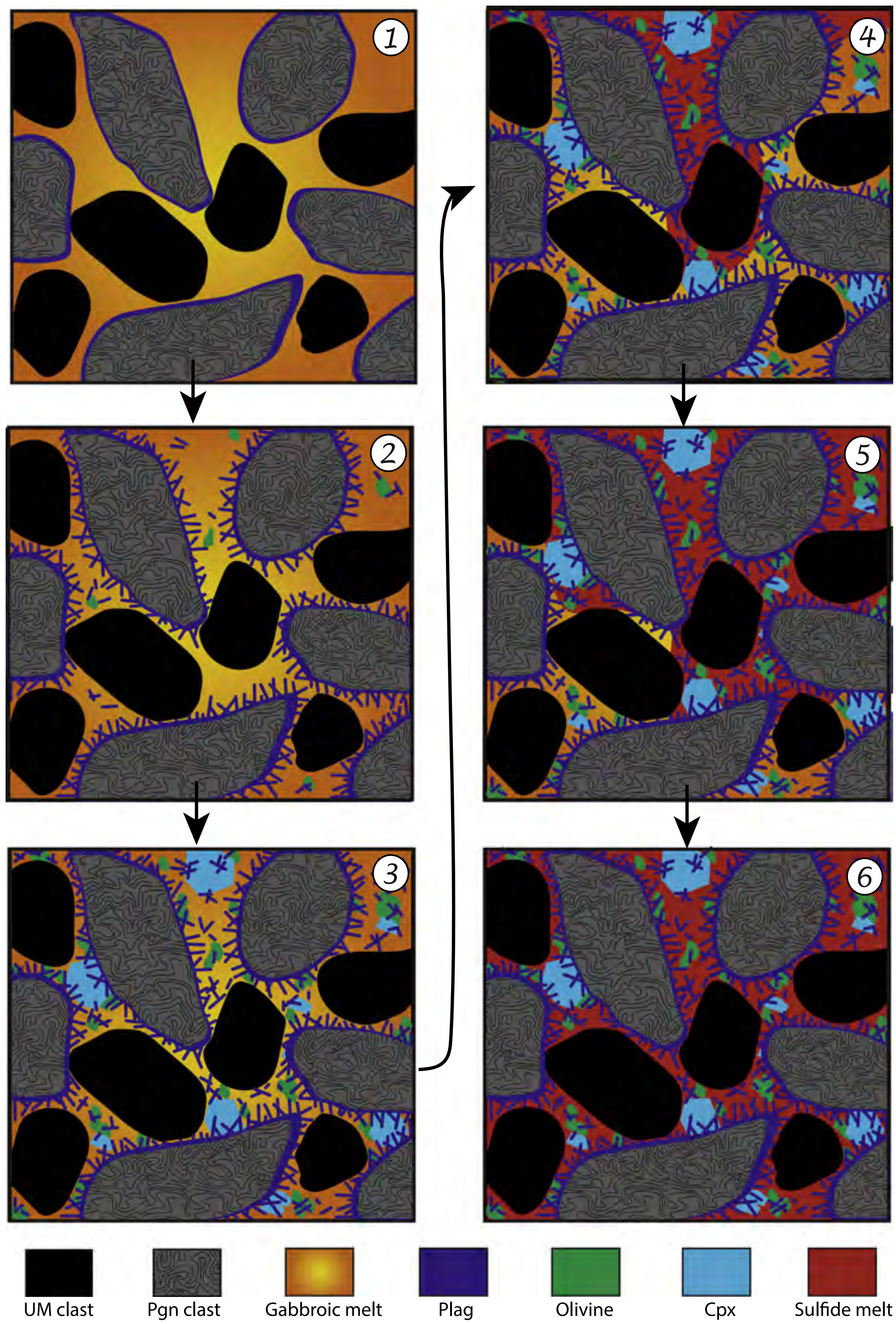

Fig. 16. Sulfide percolation cartoon. Stage a, accumulation of polymict clast assemblage at a choke point or intrusion entry point, with interstitial olivine gabbro liquid. b, growth of anorthositic reaction rim on paragneiss xenoliths, followed by nucleation of radiating plagioclase laths on the rims and growth from the interstitial silicate liquid. c, continuing crystallisation of olivine gabbro liquid to form ophitic/poikilitic olivine-plagioclase-cpx. Olivine and pyroxene grow simultaneously with plagioclase, but pyroxene grows fastest, giving rise to larger grains enclosing plagioclase. d, e, (probably overlapping with C), percolation of dense sulfide melt into residual pore space, displacing remaining silicate melt as a return flow while retaining plagioclase-olivine framework; possible remelting of silicate assemblage at plagioclase-olivine-clinopyroxene eutectic; f, final solidification of silicate and sulfide liquids.

competitive growth: oikocrysts represent rapid growth from relatively few nuclei, enclosing slower–growing phases forming from a greater abundance of nuclei, as has been proposed by a number of studies (Campbell, 1978; McBirney and Noyes, 1979; Mathison, 1987; Godel et al., 2013; Barnes et al., 2016c). On these grounds, it is more likely that plagioclase, olivine and clinopyroxene crystallised simultaneously but at different relative rates of nucleation and growth.

An alternative explanation that takes into account the likelihood of a cumulus origin of the oikocrysts is partial re-melting of a previously crystallised silicate framework by heat advected into the rock by the percolating sulfide, as has been demonstrated for

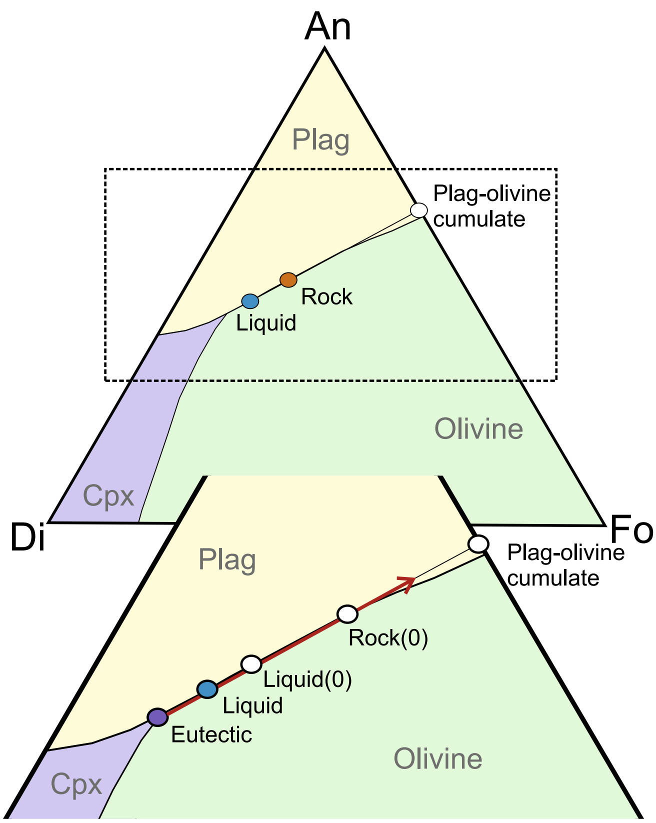

Fig. 17. Fo-Di-An phase diagram, after Presnall et al. (1978). The olivine gabbro matrix ("rock") is a mixture of accumulated olivine and plagioclase with a liquid lying along the olivine-plagioclase cotectic. With influx of the hot sulfide melt, melting begins at the eutectic; resulting partial melt is displaced and removed by the percolating sulfide, causing the remaining silicate liquid composition to migrate away from the eutectic composition. This results in preferential melting out of the clinopyroxene, leaving behind a refractory residue of olivine and plagioclase as seen in the mineralised troctolite ores.

interspinifex ores in komatiites. The process here is best understood by reference to a phase diagram, the simple ternary forsterite-diopside-anorthite (Presnall et al., 1978). The olivine gabbro matrix ("rock" in Fig. 17a) can be regarded as a mixture of accumulated olivine and plagioclase with a liquid lying along the olivine-plagioclase cotectic. If this composition solidifies partially or completely it will form an assemblage of olivine, plagioclase and clinopyroxene, i.e. the olivine gabbro. With the influx of the hot sulfide melt, melting begins at the eutectic and the resulting partial melt is displaced and removed by the percolating sulfide, causing the remaining silicate liquid composition to migrate away from the eutectic composition (Fig. 17b). This will result first in melting out of the clinopyroxene, leaving behind a refractory residue of olivine and plagioclase, forming the framework to the sulfidic troctolite. This process gives rise to the distinctive mineralised troctolite as illustrated in Fig. 4. If percolation takes places with less extensive re-melting, at a stage as in Fig. 16c, or at a late stage of solidification, then the percolating sulfide liquid flows around and preserves earlier formed clinopyroxene oikocrysts giving rise to leopard textures. Depending on the relative extent of sulfide percolation and partial re-melting at the point at which the sulfide liquid has largely solidified, the process may arrest at different stages as indicated by Fig. 16 d, e and f, and as recorded in the spectrum of textures observed (Fig. 15).

This model differs in a number of respects from that proposed by Evans-Lamswood et al. (2000), who considered the sulfide matrix breccias to be injected up the feeder dyke system as sulfide-rich slurries. The leopard-texture-defining clinopyroxene oikocrysts were regarded as having grown after emplacement from a sulfide-rich matrix by "pushing aside" the sulfide. This texture is a key line of evidence, along with the similarity in the poikilitic texture and nature of the plagioclase framework both within and outside sulfide rich domains. Plagioclase and other silicate phases could not plausibly have grown from the sulfide melt; furthermore the textural similarity argues strongly that this phase of silicate growth pre-dates the introduction of the sulfide component. The textural relationship of the oikocrysts to the sulfide, and particularly the observation common to a number of other deposits that pyroxene oikocrysts in disseminated and net-textured ores are characteristically free of sulfide inclusions (Barnes et al., 2017), is a strong line of evidence for the early, cumulus-stage development of oikocrysts. The final emplacement of the sulfide liquid into its present disposition must have been a relatively low-energy, passive process in order to preserve the delicate interconnected plagioclase framework outside the oikocrysts.

The rate of the process is limited by the flow velocity of the more viscous liquid phase, i.e. by the upward percolation rate of the displaced silicate melt. Once a network of percolating sulfide and silicate melt-filled paths is established, then percolation can be approximated as a Darcy's Law problem where melt migration flux is a function of the driving differential pressure generated by the density difference between silicate and sulfide melt, the viscosity of the silicate melt and the intrinsic permeability of the solid medium. Making an estimate of the permeability of the clast framework as approximately that of a coarse gravel or highly fractured rock, around 10^{-7} to 10^{-9} m^2 (10^6 to 10^8 millidarcys), and assuming a silicate melt viscosity of 100 Pa s, and silicate and sulfide melt densities of 2700 and 4500 kg/m^3, the Darcy equation predicts melt fluxes of the order of 10^{-6} to 10^{-8} m^3/s, which equates to flushing approximately 1 vertical metre of ~10% porosity breccia with migrating melt on a time scale between a few days to 2 years. Hence, the process is rapid compared with the time scale of tens to thousands of years for cooling and solidifying the host intrusions (Robertson et al., 2015).

5.3. Why are massive ores inclusion free?

A distinctive feature of the Ovoid at Voisey's Bay is the sharp cutoff between inclusion-rich breccias beneath and the almost completely inclusion-free nature of the overlying massive ores themselves. A similar relationship exists in a number of komatiite-associated deposits, notably the Silver Swan orebody at Black Swan, Western Australia. At Silver Swan, the base of the orebody is marked by a 2–5 m thick infiltration-melting zone with abundant xenolith and disaggregated xenomelt inclusions in sulfide; this zone is overlain by up to 10 m of extremely pure, inclusion-free massive sulfide (Dowling et al., 2004; Barnes et al., 2016b). The interpretation put on this relationship by Dowling et al. (2004) is that silicate inclusions ascend very rapidly due to their very high buoyancy once they become physically detached from the footwall rocks; estimates of Stokes Law ascent velocities for cm to dm sized clasts in dense, low viscosity sulfide liquid are in the 1–10 ms^{-1} range. Similarly, paragneiss or gabbro xenoliths would be expected to float very rapidly to the top of the Ovoid sulfide liquid pool as soon as they became completely surrounded by sulfide melt. The top contact of the breccia zone according to this explanation is a mechanical boundary where the silicate clasts are still effectively cemented together by interstitial silicate melt. Once this cement has been extensively displaced by sulfide at the top of the breccia pile, the clasts are free to float. A similar relationship has also been observed in the komatiite-associated Moran shoot at Kambalda, where "blobs" of basalt derived from melting the footwall accumulate as a "scum" at the top of a pool of

Please cite this article in press as: Barnes, S.J., et al. Textural development in sulfide-matrix ore breccias in the Voisey's Bay Ni-Cu-Co deposit, Labrador, Canada. Ore Geology Reviews (2017), http://dx.doi.org/10.1016/j.oregeorev.2017.03.019

inclusion-free massive sulfide (Staude et al., 2016, 2017, this volume).

5.4. Origin of the hydrous phases

As noted above and shown particularly in Fig. 4, biotite characteristically forms as rims between plagioclase and sulfide, and hornblende or hornblende-orthopyroxene symplectites form between olivine and sulfide. Plagioclase-biotite contacts are commonly corroded and lack the fine rim of clear plagioclase that usually surrounds the cloudy core. This very consistent textural relationship (Figs. 4, 8) suggests that this generation of biotite is forming as a replacement of plagioclase. However, it is not clear how to write a reaction that can describe this in terms of a sulfide-plagioclase reaction, given that these phases have no components in common other than a very small amount of Fe in the plagioclase.

The first possibility to consider is that the biotite represents a trace of the last vestiges of low-temperature silicate melt being squeezed or driven by volatile overpressure out of the silicate component (clasts or matrix) in the final stages of solidification. This stage would probably be roughly over the same temperature range as the late stages of solidification of the sulfide liquid. Silicate melt would preferentially wet silicate surfaces (Mungall and Su, 2005; Barnes et al., 2017) and hence might be expected to wick along the sulfide-silicate contacts. However, if this were the explanation then other incompatible components such as P and Ti would be expected to be strongly associated with the biotite and to be preferentially located along plagioclase-sulfide contacts. XRF maps of Ti and P, such as that in Fig. 10C, show that while there is a tendency for Ti and P bearing phases to be located close to clast margins, they tend to form as euhedral ilmenite and apatite grains within the outer portions of the sulfide, probably as outgrowths from the edge of the clasts (see also Fig. 4G), and not in close association with biotite (note the lack of correspondence between biotite, apatite and ilmenite in Fig. 10C). The implication is that these phases formed before displacement of silicate melt by sulfide.

An alternative hypothesis is that the biotite did indeed form by reaction between plagioclase, sulfide and a late stage volatile phase, according to reactions such as…

$$\underset{\text{(in plag)}}{2KAlSi_3O_8} + \underset{\text{(from sulfide)}}{6FeS} + 8H_2O = \underset{\text{(biotite)}}{2KFe_3AlSi_3O_{10}(OH)_2} + \underset{\text{(fluid)}}{6H_2S} \qquad (1)$$

This raises the possibility that the volatile component of the biotite may have been derived from the sulfide liquid itself. The volatile content of sulfide liquids remains largely unknown owing to the difficulty of measuring it experimentally. However, there are a number of lines of evidence to suggest that sulfide liquids may exsolved an aqueous volatile phase during the late stages of solidification. The Cu-rich footwall veins at Sudbury are commonly surrounded by m-scale haloes of PGE enrichment associated with secondary hydrous phases (Farrow and Watkinson, 1997; Hanley et al., 2004; Hanley and Bray, 2009). Wykes and Mavrogenes (2005) report experimental evidence for significant lowering of sulfide melting temperatures in the presence of water, and argue that this implies solution of water in the sulfide melt, albeit in compositions very different from typical magmatic sulfide liquids. Experimental evidence (Mungall and Brenan, 2003) also points to solubility of thousands of ppm levels of halogens in sulfide melts. Hence, the sulfide melt could supply the Fe and water and the plagioclase the Al, K and Si. The main problem is whether the plagioclase could supply enough K. Pertinent to this question is the observation that the plagioclase-biotite reaction rims are mainly developed on plagioclase formed at the margins of paragneiss xenoliths, and less commonly on the margins of gabbro xenoliths, as shown in Fig. 10B and Fig. 6C. This suggests that the K may be derived from last-gasp K-enriched partial melts of the xenoliths. Against this, it is evident from several of the XRF images that the biotite content of the ultramafic clasts is generally higher than that of the paragneiss, with the exception of some more biotite-rich paragneiss clasts such as that in sample ED19 (Fig. 10). A late stage magmatic replacement origin for the biotite is also indicated by the formation of biotite overgrowths on previously deformed plagioclase grains, as shown in Fig. 8F. Late-stage fluid-mediated reaction between sulfide and plagioclase in proximity to metasediment clasts is therefore our favoured explanation, but alternative mechanisms may exist. Regardless of the precise mechanism, it is clear from the very consistent textural relationships that the biotite-plagioclase rims represent the final stages of crystallisation, after displacement of silicate melt by sulfide melt, and cannot be used to argue for the presence of a co-existing volatile fluid phase during the initial emplacement of the breccia fragments.

5.5. When and where did the refractory mineralogy in the paragneiss clasts form?

The distinctive highly refractory mineralogy of the hercynite-bearing paragneiss clasts is a consequence of extensive partial melt extraction from original Tasuiyak gneiss protoliths, containing garnet, sillimanite, biotite, feldspar and quartz, combined with extensive reaction with assimilating magma to convert corundum to hercynite (Li and Naldrett, 2000; Mariga et al., 2006b). The most extreme product of the melt extraction process is the formation of the anorthositic rinds. Li and Naldrett (2000) noted that the hercynite reaction was more advanced progressively upward in the system from the Reid Brook Zone to the Eastern Deeps. Li and Naldrett (2000) concluded that the reaction proceeded during upward transport of the clasts by the same magma that transported the sulfides. A possible "clast nursery" has since been identified in the Western Deeps intrusion beneath the Reid Brook Zone and could have been the source.

We question some aspects of this interpretation on the basis of consideration of time scales, and also on the basis of our detailed observations combined with those of Li and Naldrett (2000). Considering time scales first, the conversion of corundum to hercynite must have been driven by solid state diffusion through the clasts. This is a very slow process compared with the time scale of magma transport. Mariga et al. (2006b) calculated approximate equilibration times of 3000–23,000 years, compared with expected magma transport rates of the order of cm to m per second. On the other hand, dissolution rates of cm-scale felsic inclusions in mafic magmas should be very fast, of the order of minutes to hours (Robertson et al., 2015). This apparent paradox indicates that the mineralogy of the clasts is likely to have been developed within a thermal aureole rather than after incorporation of the clast into the assimilating magma. The refractory mineralogy developed before clast incorporation, such that by the time the clast had been incorporated they were already unreactive. The transporting magma was already plagioclase saturated; a clast composed largely of plagioclase and corundum could no longer either melt or dissolve and acted as an inert passenger.

A second related observation is the lack of chemical haloes within the silicate matrix immediately surrounding the paragneiss clasts. As we have seen, the texture and mineralogy of the olivine gabbro matrix to the breccias is essentially identical to that of the vari-textured olivine gabbro without clasts, and mm to cm scale geochemical haloes around the clasts are subtle at best. Aside from the outer rind of pure plagioclase in the paragneiss clasts, the reaction rims we observe are primarily between the crystallisation products of the matrix and the sulfide, rather than between silicate matrix and clast, although it has been noted above that the biotite rims between sulfide and matrix plagioclase tend to be more abundant around the paragneiss clasts than around the ultramafic or olivine gabbro clasts. The implication is that much of the melt extraction from paragneiss took place "off-stage" prior to deposition of the clasts in the deposit. This argues against localized sulfide saturation in response to silicification of the olivine gabbro magma. The hercynite replacement could have taken place pre- or post-incorporation, but is unlikely to have taken place during transport. The more advanced reaction in the Eastern Deeps relative to Reid Brook setting could simply reflect a longer time to equilibrate with the matrix magma at slower cooling rates in the large Eastern Deeps intrusion relative to the thin Reid Brook dyke.

5.6. Relative timing of sulfide and breccia fragment emplacement

The model proposed here raises the possibility that the silicate rock fragment and sulfide liquid components of the Voisey's Bay ores do not necessarily have to have been emplaced simultaneously, or even from the same source. There is however a well-established spatial association between sulfides and externally derived breccia clasts at Voisey's Bay. This association extends from the Reid Brook Zone through the Western Extension to the Mini-ovoid and Ovoid, and is also evident in the Southeastern Extension and Eastern Deepszones.. This critical spatial association must be explained by a genetic model. The same relationship between sulfide ores and country rock xenoliths is observed in many other mafic-hosted deposits including those at Noril'sk (Naldrett, 2004).

It is possible that slurries of silicate and sulfide melt and rock fragments could have been emplaced simultaneously, with subsequent percolation-migration of sulfide liquid giving rise to the observed array of textures. However, there is an alternative explanation that the breccia fragments and sulfide liquid may have been

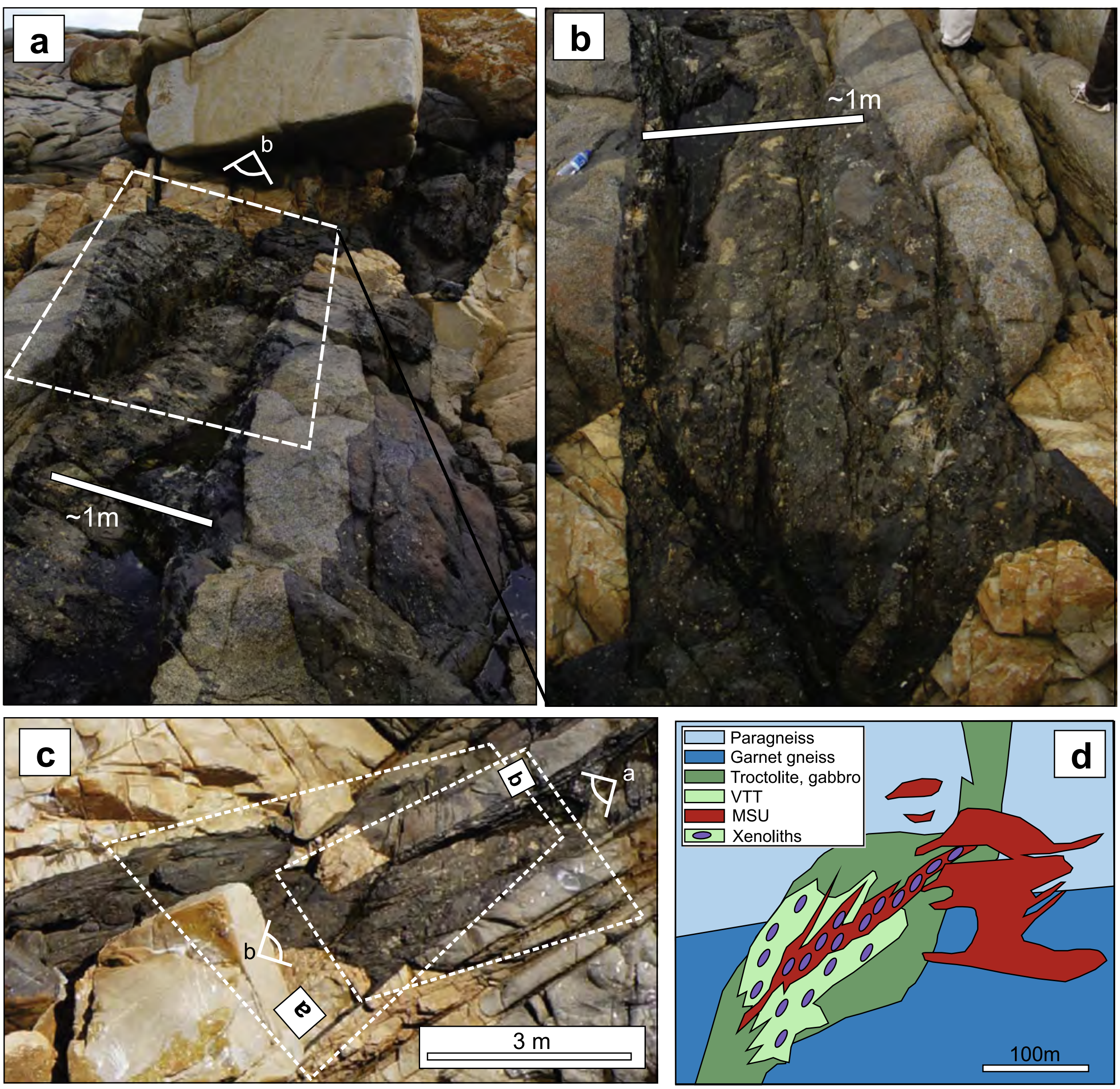

Fig. 18. a,b, Xenoliths concentrated in a step-over structure between two segments of an alkali dolerite dyke emplaced into granites at Bingie Bingie point, near Moruya, New South Wales. Xenolith concentration drops off rapidly within 2–3 metres away from the step-over. c, Aerial photomontage *ortho*-image of section of the Bingie Bingie dyke after Cruden et al. (2016) showing location of images a and b (note that a and b are viewed from opposite directions – angle symbol indicates point of view). d, simplified geometry of the Reid Brook Zone deposit at Voisey's Bay, after Lightfoot and Evans-Lamswood (2015), showing location of sulfide rich and poor breccias and cross cutting massive sulfides associated with a dyke step-over.

derived separately, and owe their current spatial association to the presence of effective choke-points within the conduit system, as proposed by Barnes et al. (2016b).

As an example of such a choke point, Fig. 18 shows a step-over or "bridge" between two dyke sections in a xenolith bearing alkali dolerite dyke at Bingie Bingie Point on the coast of New South Wales (Cruden et al., 2016). A high concentration of xenoliths is found in the neck of the step-over, implying that this constriction acted as a "strainer" that filtered out xenoliths as the magma flowed past. The Reid Brook Zone at Voisey's Bay has been interpreted by Saumur and Cruden (2015) as such a structure. Sulfide liquid droplets being transported through the dyke network could have been simultaneously concentrated at such choke points; furthermore, dense sulfide liquid draining back down the conduit during periods of stagnation or intermittent back flow (Barnes et al., 2016b) could have been trapped by breccia log-jams acting as a kind of filter bed. In the case of the Reid Brook zone, the ore is hosted within a small inclined chonolith extending along the structural intersection, and we would interpret the sulfide transport as being dominantly lateral along this rather than from the narrow dyke above.

The textures observed in this study do not provide conclusive evidence for the ultimate derivation of the clasts or the sulfide. Arguing against independent derivation of clasts and sulfides is the lack of sulfide-free breccias, or massive sulfides without silicate rock fragments, anywhere in the Voisey's Bay system, tending to argue that the sulfides and rock fragments were derived from the same source and emplaced together. However, our observations provide a key line of evidence that the final disposition of the sulfide involved downward drainage of sulfide through the self-supporting matrix of pre-existing, relatively sulfide-poor intrusion breccias. Whatever the ultimate derivation of the sulfide liquid, its final emplacement direction as recorded in the ore textures was downward. Future models should consider dynamic multi-stage dynamic process involving both upward and downward flow in recharged magmatic plumbing systems, as commonly observed during prolonged basaltic eruptions (Orr et al., 2015).

6. Conclusions

The array of silicate-sulfide textures in the Voisey's Bay ore breccias is interpreted as the result of a two stage process: accumulation of a "sludge" (Naldrett, pers. comm. 2016) of partially molten rock fragments derived both from country rocks and the intrusive complex itself, possibly concentrated at choke points in the magma flow pathway; followed by downward percolation of sulfide melt into the interstitial space between the mostly refractory silicate clasts, with simultaneous upward displacement of the original interstitial silicate melt. This process is closely analogous to the formation of net-textured ores and particularly inter-spinifex ores in komatiitic settings as discussed in detail by Barnes et al. (2017). This model explains a number of previously unexplained features of the Voisey's Bay breccias, particularly the persistence of delicate plagioclase crystal frameworks within the sulfide domains, and the similarity of this plagioclase framework between sulfide-rich areas, clinopyroxene oikocrysts and weakly mineralised or barren olivine gabbros.

The wide diversity of textures can be explained by a simple interplay of two variables: the abundance and lithological makeup of the clast population; and the timing of sulfide infiltration relative to the degree of crystallisation of the inter-clast silicate melt component. Where the silicate melt was already largely crystalline, preferential remelting of the silicate component begins with melting at the eutectic plagioclase-olivine-pyroxene eutectic, resulting in some cases in complete removal of the clinopyroxene component leaving behind net-textured material with sulfide interstitial to plagioclase and olivine. The same texture may have been generated where sulfide migration takes place while the silicate melt was fractionating along the plagioclase-olivine cotectic at temperatures above the appearance of clinopyroxene. Where sulfide penetrates early, the result is strongly interconnected channelways of nearly pure inclusion-poor sulfide. Where melting at the eutectic was incomplete, preservation of early-formed clinopyroxene oikocrysts gave rise to leopard textures. Strongly interconnected 3D sulfide networks form at multi-metre scale where the inter-clast porosity was high and the degree of crystallinity low.

This model is distinct from previous interpretations that the Voisey's Bay breccias were emplaced as upward-transported slurries of silicate and sulfide liquid with abundant entrained rock fragments, and solidified in situ as such. We propose an alternative scenario where sulfide-poor rock fragments become trapped at choke points such as dyke step-overs, and form mechanical traps for sulfide liquid migrating back down the vertical conduit system from above while the core of the dyke remains primarily molten and clast-poor. This interpretation says nothing about the original derivation of the sulfide liquid; it may have been transported as liquid droplets along with the breccia fragments, segregated into pools in close proximity, and then drained back into the pore space of the breccias (Barnes et al., 2016b). Furthermore at this stage there is no indication of how far the sulfides may have migrated. Detailed spatial studies of sulfur isotopes may provide the critical evidence (Ripley et al., 1999; Ripley and Li, 2002). The key observation is that the final disposition of sulfide in the ore is due to this late stage drainage, taking place under relatively placid conditions, and does not reflect the original makeup of a mechanically transported slurry.

The Voisey's Bay ore breccias lie on a continuum of magmatic sulfide ore textures that reflect interactions between sulfide melts, their host silicate magmas, and the wall rocks of the containing magma pathways. They represent a particular kind of infiltration-melting front reflecting the potential of hot, dense, low viscosity sulfide liquids to penetrate and remelt underlying silicate rocks. Similar examples may be found in many different deposits, both komatiite hosted (Staude et al., 2016, 2017) and mafic-hosted. The combination of microbeam XRF mapping and 3D tomography employed here is a powerful technique for unlocking the mechanisms involved.

Acknowledgments

We thank Vale for access to samples and permission to undertake this work under the terms of a research agreement. We thank Dawn Evans-Lamswood, Danny Mulrooney, Sheldon Pittman, and Lisa Gibson for their help. Steve Beresford is thanked for the loan of some important samples, a review of an early draft and for helpful discussions. Belinda Godel reviewed an early draft and assisted with 3D imagery. We thank Sandy Cruden for the UAV image used in Fig. 18. Some of the images presented here were collected on the X-ray fluorescence microscopy beam line at the Australian Synchrotron, Clayton, Victoria, Australia, and we acknowledge the assistance of Daryl Howard, David Paterson, Martin De Jonge and Kathryn Spiers. We acknowledge financial support for this facility from the Science and Industry Endowment Fund (SIEF). We thank the National Geosequestration Lab and Lionel Esteban for access to the medical CT scanner at CSIRO-ARRC, Michael Verrall for assistance with the Bruker Tornado™ desktop XRF mapper and iVEC and Andrew Squelch for access to and assistance with computer hardware and Avizo image processing software. This work was supported by resources provided by the Pawsey Supercomputing Centre with funding from the Australian Government and the

Government of Western Australia. SJB and MLV are funded by the CSIRO Research Plus Science Leader program.

Appendix A. Supplementary data

Supplementary data associated with this article can be found, in the online version, at http://dx.doi.org/10.1016/j.oregeorev.2017.03.019.

References

Arcuri, T., Ripley, E.M., Hauck, S.A., 1998. Sulfur and oxygen isotope studies of the interaction between pelitic xenoliths and basaltic magma at the Babbitt and Serpentine Cu-Ni deposits, Duluth Complex, Minnesota. Econ. Geol. 93, 1063–1075.

Barnes, Stephen J., Beresford, S.W., Le Vaillant, M., 2016a. Interspinifex Ni sulfide ore from the Coronet Shoot, Kambalda: characterisation using microbeam XRF mapping and 3D X-ray computed tomography. Econ. Geol. 111, 1509–1517.

Barnes, Stephen J., Cruden, A.R., Arndt, N.T., Saumur, B.M., 2016b. The mineral system approach applied to magmatic Ni-Cu-PGE sulphide deposits. Ore Geol. Rev. 76, 296–316.

Barnes, Stephen J., Mole, D.R., Le Vaillant, M., Campbell, M., Verrall, M., Roberts, M., Evans, N.J., 2016c. Poikilitic textures, heteradcumulates and zoned orthopyroxenes in the Ntaka Ultramafic Complex, Tanzania: implications for crystallisation mechanisms of oikocrysts. J. Petrol. 57, 1171–1198.

Barnes, Stephen J., Mungall, J.E., Le Vaillant, M., Godel, B., Lesher, C.M., Holwell, D.A., Lightfoot, P.C., Krivolutskaya, N.A., Wei, B., 2017. Sulfide-silicate textures in magmatic Ni-Cu-PGE sulfide ore deposits. 1. Disseminated and net-textured ores. Am. Mineral. 102, 473–506.

Campbell, I.H., 1978. Some problems with the cumulus theory. Lithos 11, 311–323.

Chung, H.-Y., Mungall, J.E., 2009. Physical constraints on the migration of immiscible fluids through partially molten silicates, with special reference to magmatic sulfide ores. Earth Planet. Sci Lett. 286, 14–22.

Cruden, A.R., Vollgger, S., Dering, G., Micklethwaite, S., 2016. High spatial resolution mapping of dykes using unmanned aerial vehicle (UAV) photogrammetry: new insights on emplacement processes. Acta Geol. Sinica (Engl. Ed.) 90 (Supp 1), 52–53.

Dowling, S.E., Barnes, Stephen J., Hill, R.E.T., Hicks, J., 2004. Komatiites and nickel sulfide ores of the Black Swan area, Yilgarn Craton, Western Australia. 2. Geology and genesis of the orebodies. Mineral. Depos. 39, 707–728.

Evans-Lamswood, D.M., Butt, D.P., Jackson, R.S., Lee, D.V., Muggridge, M.G., Wheeler, R.I., Wilton, D.H.C., 2000. Physical controls associated with the distribution of sulfides in the Voisey's Bay Ni-Cu-Co deposit, Labrador. Econ. Geol. 95, 749.

Farrow, C.E.G., Watkinson, D.H., 1997. Diversity of precious-metal mineralization in footwall Cu-Ni-PGE deposits, Sudbury, Ontario – implications for hydrothermal models of formation. Can. Mineral. 35, 817–839.

Fisher, L.A., Fougerouse, D., Halfpenny, A., Ryan, C.G., Micklethwaite, S., Hough, R.M., Cleverley, J.S., Gee, M., Paterson, D., Howard, D., 2015. Fully quantified, multi-scale element mapping of mineral system samples using the Maia detector array: recognizing chemical variation on micron to cm scales. Mineral. Depos. 50, 665–674.

Godel, B., Barnes, Sarah.- .J., Maier, W.D., 2006. 3-D distribution of sulphide minerals in the Merensky Reef (Bushveld Complex, South Africa) and the J-M Reef (Stillwater Complex, USA) and their relationship to microstructures using X-ray computed tomography. J. Petrol. 47, 1853–1872.

Godel, B.M., Barnes, Stephen J., Gurer, D., Austin, P., Fiorentini, M.L., 2013. Chromite in komatiites: 3D morphologies with implications for crystallization mechanisms. Contrib. Mineral. Petrol. 165, 173–189.

Groves, D.I., Korkiakoski, E.A., McNaughton, N.J., Lesher, C.M., Cowden, A., 1986. Thermal erosion by komatiites at Kambalda, Western Australia and the genesis of nickel ores. Nature 319, 136–139.

Hanley, J.J., Bray, C.J., 2009. The trace metal content of amphibole as a proximity indicator for Cu-Ni-PGE mineralization in the footwall of the Sudbury Igneous Complex, Ontario, Canada. Econ. Geol. 104, 113–125.

Hanley, J.J., Mungall, J.E., Bray, C.J., Gorton, M.P., 2004. The Origin of Bulk and Water-Soluble Cl and Br Enrichments in Ore-Hosting Sudbury Breccia in the Fraser Copper Zone, Strathcona Embayment, Sudbury, Ontario, Canada. Can. Mineral. 42, 1777–1798.

Huminicki, M.A.E., Sylvester, P.J., Shaffer, M., Wheeler, R.I., 2012. Systematic and integrative ore characterization of massive sulfide deposits: an example from Voisey's bay Ni-Cu-Co ovoid orebody. Explor. Min. Geol. 20, 53–86.

Li, C., Lightfoot, P.C., Amelin, Y.V., Naldrett, A.J., 2000. Contrasting petrological and geochemical relationships in the Voisey's Bay and Mushuau intrusions, Labrador, Canada; implications for ore genesis. Econ. Geol. 95, 771–799.

Li, C., Naldrett, 2000. Melting reactions of gneissic inclusions with enclosing magma at Voisey's Bay, Labrador, Canada; implications with respect to ore genesis. Econ. Geol. 95, 801–814.

Lightfoot, P.C., 2016. Nickel Sulfide Ores and Impact Melts. Elsevier.

Lightfoot, P.C., Evans-Lamswood, D.M., 2015. Structural controls on the primary distribution of mafic–ultramafic intrusions containing Ni–Cu–Co–(PGE) sulfide mineralization in the roots of large igneous provinces. Ore Geol. Rev. 64, 354–386.

Lightfoot, P.C., Keays, R.R., Evans-Lamswood, D., Wheeler, R., 2012. S saturation history of Nain plutonic suite mafic intrusions; origin of the Voisey's Bay Ni-Cu-Co sulfide deposit, Labrador, Canada. Mineral. Depos. 47, 23–50.

Lightfoot, P.C., Naldrett, A.J., 1999. Geological and geochemical relationships in the Voisey's Bay intrusion Nain Plutonic Suite Labrador, Canada. Geological Association of Canada Short Course Notes 13, 1–31.

Mariga, J., Ripley, E.M., Li, C., 2006a. Oxygen isotopic studies of the interaction between xenoliths and mafic magma, Voisey's Bay Intrusion, Labrador, Canada. Geochim. Cosmochim. Acta 70, 4977–4996.

Mariga, J., Ripley, E.M., Li, C., 2006b. Petrologic evolution of gneissic xenoliths in the Voisey's Bay Intrusion, Labrador, Canada: Mineralogy, reactions, partial melting, and mechanisms of mass transfer. Geochem., Geophys., Geosyst. 7.

Mathison, C.I., 1987. Pyroxene oikocrysts in troctolitic cumulates; evidence for supercooled crystallisation and postcumulus modification. Contrib. Mineral. Petrol. 97, 228.

McBirney, A.R., Noyes, R.M., 1979. Crystallization and layering in the Skaergaard Intrusion. J. Petrol. 20, 487–554.

Mungall, J.E., Brenan, J.M., 2003. Experimental evidence for the chalcophile behavior of the halogens. Can. Mineral. 41, 207–220.

Mungall, J.E., Su, S., 2005. Interfacial tension between magmatic sulfide and silicate liquids: constraints on the kinetics of sulfide liquation and sulfide migration through silicate rocks. Earth Planet. Sci Lett. 234, 135–149.

Naldrett, A.J., 2004. Magmatic Sulphide Deposits. Oxford University Press, New York.

Naldrett, A.J., Asif, M., Li, C., 2000. The composition of mineralization of the Voisey's Bay Ni-Cu sulfide deposit, with special reference to platinum-group elements. Econ. Geol. 95, 845–865.

Naldrett, A.J., Keats, H., Sparkes, K., Moore, R., 1996. Geology of the Voisey's Bay Ni-Cu-Co deposit, Labrador, Canada. Exploration Mining Geol. 5, 69–179.

Orr, T.R., Poland, M.P., Patrick, M.R., Thelen, W.A., Sutton, A.J., Elias, T., Thornber, C. R., Parcheta, C., Wooten, K.M., 2015. Kı̄lauea's 5–9 March 2011 Kamoamoa Fissure Eruption and Its Relation to 30+ Years of Activity From Pu'u 'Ō 'ō. In: Carey, R.J., Cayol, V., Poland, M., Weis, D. (Eds.), Hawaiian Volcanoes: From Source to Surface, Geophysical Monograph 208. John Wiley and Sons, American Geophysical Union, pp. 393–420.

Paterson, D., de Jonge, M.D., Howard, D.L., Lewis, W., McKinlay, J., Starritt, A., Kusel, M., Ryan, C.G., Kirkham, R., Moorhead, G., Siddons, D.P., 2011. The X-ray Fluorescence Microscopy Beamline at the Australian Synchrotron. Proc. Aust. Inst. Phys. 1365, 219–222.

Perring, C.S., Barnes, Stephen J., Hill, R.E.T., 1995. The physical volcanology of komatiite sequences from Forrestania, Southern Cross Province, Western Australia. Lithos 34, 189–207.

Pina, R., Lunar, R., Ortega, L., Gervilla, F., Alapieti, T., Martinez, C., 2006. Petrology and geochemistry of mafic-ultramafic fragments from the Aguablanca Ni-Cu Ore Breccia, Southwest Spain. Econ. Geol. 101, 865–881.

Prendergast, M.D., 2001. Komatiite-hosted Hunters Road nickel deposit, central Zimbabwe: physical volcanology and sulfide genesis. Aust. J. Earth Sci. 48, 681–694.

Presnall, D.C., Dixon, S.A., Dixon, J.R., O'Donnell, T.H., Brenner, N.L., Schrock, R.L., Dycus, D.W., 1978. Liquidus phase relations on the join diopside-forsterite-anorthite from 1 atm to 20 kbar; their bearing on the generation and crystallization of basaltic magma. Contrib. Mineral. Petrol. 66, 203–220.

Ripley, E.M., Alawi, J.A., 1988. Petrogenesis of pelitic xenoliths at the Babbitt Cu-Ni deposit, Duluth Complex, Minnesota, U.S.A. Lithos 21, 143–159.

Ripley, E.M., Li, 2002. Paragneiss assimilation in the genesis of magmatic Ni-Cu-Co sulfide mineralization at Voisey's Bay, Labrador; delta (super 34# Sdelta #super 13) C, and Se/S evidence. Econ. Geol. 97, 1307.

Ripley, E.M., Li, C., 2011. A Review of Conduit-Related Ni-Cu-(PGE) Sulfide Mineralization at the Voisey's Bay Deposit, Labrador, and the Eagle Deposit, Northern Michigan. In: Li, C., Ripley, E.M. (Eds.), Magmatic Ni-Cu and PGE deposits: geology, geochemistry and genesis. Reviews in Economic Geology 17. Society of Economic Geologists, Littleton, pp. 181–197.

Ripley, E.M., Park, Y.-R., Li, C., Naldrett, A.J., 1999. Sulfur and oxygen isotopic evidence of country rock contamination in the Voisey's Bay Ni-Cu-Co deposit, Labrador, Canada. Lithos 47, 53–68.

Robertson, J.C., Barnes, Stephen J., Le Vaillant, M., 2016. Dynamics of magmatic sulphide droplets during transport in silicate melts and implications for magmatic sulphide ore formation. J. Petrol. 56, 2445–2472.

Robertson, J.C., Ripley, E.M., Barnes, Stephen J., Li, C., 2015. Sulfur liberation from country rocks and incorporation in mafic magmas. Econ. Geol. 110, 1111–1123.

Ryan, B., 2000. The Nain-Churchill boundary and the Nain plutonic suite: a regional perspective on the geologic setting of the Voisey's Bay Ni-Cu-Co deposit. Econ. Geol. 95, 703–724.

Ryan, C.G., Kirkham, R., Hough, R.M., Moorhead, G., Siddons, D.P., de Jonge, M.D., Paterson, D.J., De Geronimo, G., Howard, D.L., Cleverley, J.S., 2010. Elemental X-ray imaging using the Maia detector array: The benefits and challenges of large solid-angle. Nucl. Instrum. Methods Phys. Res. Sect., A 619, 37–43.

Ryan, C.G., Siddons, D.P., Kirkham, R., Li, Z.Y., de Jonge, M.D., Paterson, D.J., Kuczewski, A., Howard, D.L., Dunn, P.A., Falkenberg, G., Boesenberg, U., De Geronimo, G., Fisher, L.A., Halfpenny, A., Lintern, M.J., Lombi, E., Dyl, K.A., Jensen, M., Moorhead, G.F., Cleverley, J.S., Hough, R.M., Godel, B., Barnes, Stephen J., James, S.A., Spiers, K.M., Alfeld, M., Wellenreuther, G., Vukmanovic, Z., Borg, S., 2014. Maia X-ray fluorescence imaging: capturing detail in complex natural samples. J. Phys.: Conference Series, 012002.

Samalens, N., Barnes, Sarah.- .J., Sawyer, E.J., 2016. The role of black shales as a source of sulfur and semimetals in magmatic nickel-copper deposits: Example from the Partridge River Intrusion, Duluth Complex, Minnesota, USA. Ore. Geol. Rev.

Saumur, B.M., Cruden, A.R., 2015. On the emplacement of the Voisey's Bay intrusion (Labrador, Canada). Geol. Soc. Amer. Bull. 128, 147–168.

Saumur, B.M., Cruden, A.R., Boutelier, D., Evans-Lamswood, D.M., 2013. Structure and Dynamics of Magmatic Ni-Cu Sulphide Deposits: Theory, Analogue Modelling and Insights From Voisey's Bay (Labrador, Canada), 13th Biennial SGA Meeting. SGA, Uppsala, Sweden.

Saumur, B.M., Cruden, A.R., Evans-Lamswood, D.M., Lightfoot, P.C., 2015. Wall-Rock Structural Controls on the Genesis of the Voisey's Bay Intrusion and its Ni-Cu-Co Magmatic Sulfide Mineralization (Labrador, Canada). Econ. Geol. 110, 691–711.

Staude, S., Barnes, Stephen J., Le Vaillant, M., 2016. Evidence of lateral thermomechanical erosion of basalt by Fe-Ni-Cu sulfide melt at Kambalda, Western Australia. Geology online.

Staude, S., Le Vaillant, M., Barnes, Stephen J., 2017. Thermomechanical excavation of ore-hosting embayments beneath komatiite lava channels: textural evidence from the Moran deposit, Kambalda Western Australia. Ore. Geol. Rev.

Wykes, J.L., Mavrogenes, J.A., 2005. Hydrous Sulfide Melting: Experimental Evidence for the Solubility of H_2O in Sulfide Melts. Econ. Geol. 100, 157–164.

Please cite this article in press as: Barnes, S.J., et al. Textural development in sulfide-matrix ore breccias in the Voisey's Bay Ni-Cu-Co deposit, Labrador, Canada. Ore Geology Reviews (2017), http://dx.doi.org/10.1016/j.oregeorev.2017.03.019